Research Square

Preprints are preliminary reports that have not undergone peer review.
They should not be considered conclusive, used to inform clinical practice,
or referenced by the media as validated information.

Westernized diet related arachidonic acid metabolism expands DNA error-prone growth factor-dependent colonic quiescent stem cells in adolescent mice

Stefanie Derer

stefanie.derer@uksh.de

Institute of Nutritional Medicine, University Hospital Schleswig-Holstein, Lübeck

Lea Christiansen

Institute of Nutritional Medicine, University Hospital Schleswig-Holstein https://orcid.org/0009-0001-0595-1425

Mohab Ragab

Department of Internal Medicine II, Klinikum rechts der Isar, TUM School of Medicine and Health, Technical University of Munich

Laura Nickel

2nd Department of Medicine, Sana Clinics Lübeck

Maren Hicken

Institute of Nutritional Medicine, University Hospital Schleswig-Holstein

Heidi Schlichting

Institute of Nutritional Medicine, University Hospital Schleswig-Holstein

Rudrik Weikamp

Institute of Nutritional Medicine, University Hospital Schleswig-Holstein, Lübeck

Franziska Schmelter

Institute of Nutritional Medicine, University Hospital Schleswig-Holstein

Daniel Margis

Institute of Nutritional Medicine, University Hospital Schleswig-Holstein, Lübeck

Stefan Mertel

Institute of Nutritional Medicine, University Hospital Schleswig-Holstein

Ines Richerzhagen

Institute of Nutritional Medicine, University Hospital Schleswig-Holstein

Henrike Wenk

Institute of Nutritional Medicine, University Hospital Schleswig-Holstein

Sebastian Tornow

Institute of Nutritional Medicine, University Hospital Schleswig-Holstein

Nele Buchmann
Institute of Nutritional Medicine, University Hospital Schleswig-Holstein
Daniel Vondran
Institute of Nutritional Medicine, University Hospital Schleswig-Holstein
Clarissa Gottschild
Institute of Nutritional Medicine, University Hospital Schleswig-Holstein
Annika Raschdorf
Institute of Nutritional Medicine, University Hospital Schleswig-Holstein
Larissa Nogueira de Almeida
Institute of Nutritional Medicine, University Hospital Schleswig-Holstein
OUTLIVE-CRC consortium
A complete list of investigators in OUTLIVE-CRC (OUTLIVE-Colorectal Cancer consortium) is provided on www.outlive-crc.uni-luebeck.de/konsortium
Timo Gemoll
Section for Translational Surgical Oncology & Biobanking, Department of Surgery, University Medical Center Schleswig-Holstein, Campus Lübeck & University of Lübeck
Lina Jegodzinski
University Hospital Schleswig-Holstein Lübeck
Darko Castven
Department of Medicine I, University Hospital Schleswig-Holstein
Jens Marquardt
University Hospital of Schleswig-Holstein https://orcid.org/0000-0002-8314-2682
Senad Divanovic
Division of Immunobiology, Cincinnati Children's Hospital Medical Center, Cincinnati, Ohio 45229 https://orcid.org/0000-0001-7538-0499
Walter Raasch
University of Lübeck, Institute for Experimental and Clinical Pharmacology and Toxicology
Christian Sina
Institute of Nutritional Medicine, University Hospital Schleswig-Holstein, Lübeck
Stefanie Derer
Institute of Nutritional Medicine, University Hospital Schleswig-Holstein, Lübeck

---

Article

Keywords:

Posted Date: March 12th, 2026

DOI: https://doi.org/10.21203/rs.3.rs-9050026/v1

License: This work is licensed under a Creative Commons Attribution 4.0 International License.
Read Full License

Additional Declarations: There is **NO** Competing Interest.

Westernized diet related arachidonic acid metabolism expands DNA error-prone growth factor-dependent colonic quiescent stem cells in adolescent mice

Lea Christiansen[1], Mohab Ragab[1,2], Laura Nickel[3,4], Maren Hicken[1], Heidi Schlichting[1], Rudrik Weikamp[1], Franziska Schmelter[1], Daniel Margis[1], Stefan Mertel[1], Ines Richerzhagen[1], Henrike Wenk[1], Sebastian Tornow[1], Nele Buchmann[1], Daniel Vondran[1], Clarissa Gottschild[1], Annika Raschdorf[1], Larissa Nogueira de Almeida[1], OUTLIVE-CRC consortium[5], Timo Gemoll[6], Lina Jegodzinski[7], Darko Castven[7], Jens U. Marquardt[7], Senad Divanovic[8,9], Walter Raasch [3,10,11], Christian Sina[1,7], Stefanie Derer[1*]

[1]Institute of Nutritional Medicine, University Hospital Schleswig-Holstein, Campus Lübeck, Lübeck, Germany;

[2]Department of Internal Medicine II, Klinikum rechts der Isar, TUM School of Medicine and Health, Technical University of Munich, Munich, Germany;

[3]Institute of Experimental and Clinical Pharmacology and Toxicology, University of Lübeck, Lübeck, Germany;

[4]2nd Department of Medicine, Sana Clinics Lübeck, Lübeck, Germany;

[5]A complete list of investigators in OUTLIVE-CRC (OUTLIVE-Colorectal Cancer consortium) is provided on www.outlive-crc.uni-luebeck.de/konsortium;

[6]Section for Translational Surgical Oncology & Biobanking, Department of Surgery, University Medical Center Schleswig-Holstein, Campus Lübeck & University of Lübeck, Lübeck, Germany;

[7]Department of Medicine I, University Hospital Schleswig-Holstein, Lübeck, Germany;

[8]Department of Pediatrics, University of Cincinnati College of Medicine, Cincinnati, OH USA;

[9]Division of Immunobiology, Cincinnati Children's Hospital Medical Center, Cincinnati, OH USA;

[10]DZHK (German Centre for Cardiovascular Research), Partner Site Hamburg/Kiel/Lübeck, Lübeck, Germany;

[11]CBBM (Centre of Brain, Behaviour and Metabolism), University of Lübeck, Lübeck, Germany.

Grant support: This work was supported by the German Federal Ministry of Education and Research (BMFTR; grant 01KD2103A within the OUTLIVE-CRC consortium). The 6-week HFD feeding experiment was funded by the German Research Foundation (DFG; IRTG1911-A6), and the 12-week HFD study was supported by the DFG to the Research Training group 1957 "Adipocyte-Brain Crosstalk", University of Lübeck. J.U.M. is supported by HORIZON-MISS-2021-CANCER-02-01 (Oncoscreen consortium).

Abbreviations: 1D, one-dimensional; 2D, two-dimensional; AA, arachidonic acid; AcCA, acylcarnitine; ACTB, actin-ß; ALOX, lipoxygenases; ALPI, alkaline phosphatase; AMPKα, AMP-activated protein kinase subunit alpha; ANOVA, analysis of variance; AOM/DSS, azoxymethane/dextran sodium sulfate; APOBR, apolipoprotein B receptor; ARRIVE, Animal Research: Reporting of In Vivo Experiments; BMI1, B lymphoma Mo-MLV insertion region 1 homolog; BSA, bovine serum albumin; CASP1, caspase 1;

CCHMC, Cincinnati Children's Hospital Medical Center; CD, control diet; cDNA, complementary deoxyribonucleic acid; CE, cholesterylester; Cer, Ceramide; CerG, glycosphingolipid; COX, cyclooxygenases; CPMG, Carr-Purcell-Meiboom-Gill; CRC, colorectal cancer; CTNNB1, catenin beta 1; DAB, 3,3'-diaminobenzidine; DAG, diacylglycerols; DAGLβ, diacylglycerol lipase beta; DEPC, diethylpyrocarbonate; DGAT1, diacylglycerol O-transferase; DMEM, Dulbecco's Modified Eagle Medium; DMSO, dimethyl sulfoxide; DNMT1, DNA methyltransferase 1; DPBS, Dulbecco's phosphate-buffered saline; DSC, deep-secretory cells; DSC, deep-secretory cells; DTT, dithiothreitol; EA, ethanolamides; EC, epithelial cell; EGF, epidermal growth factor; EGFR, epidermal growth factor receptor; ELISA, enzyme-linked immunosorbent assay; eoCRC, early onset colorectal cancer; FA, fatty acid; FCS, fetal calf serum; FFPE, formalin-fixed paraffin-embedded; flx/flx, 2lox; GCDR, Gentle Cell Dissociation Reagent; HEPES, 4-(2-hydroxyethyl)-1-piperazineethanesulfonic acid; HES1, hairy and enhancer of split-1; HFD, high-fat diet; HMGCS1, 3-hydroxy-3-methylglutaryl-CoA synthase 1; HOPX, homeodomain only protein X; HRP, horseradish peroxidase; IGF2R, insulin growth factor 2 receptor; IHC, immunohistochemistry; IL6, interleukin 6; IL6R, interleukin 6 receptor; INSR, insulin receptor; IQR, interquartile range; ISC, intestinal stem cell; ISC, intestinal stem cells; IVDr, in vitro diagnostic research; KLF4, krueppel-like factor 4; KRT19, keratin 19; LA, linoleic acid;LC/MS, liquid chromatography-mass spectrometry; LC-MS/MS, liquid chromatography-tandem mass spectrometry; LDHA, lactate dehydrogenase A; LDLR, low density lipoprotein receptor; LGR5, leucine-rich repeat-containing G protein-coupled receptor 5; LPC, lysophosphatidylcholine; LPL, lipoprotein lipase; LRIG1, leucine-rich repeats and immunoglobulin-like domains protein 1; LSD, least significant difference; LTA4, leukotriene A4; LTB5, Leukotriene B5; LYZ, lysozyme; MAPK, mitogen-activated protein kinase; MC, mature cell; MC, mature cell; MetS, metabolic syndrome; MMR, DNA mismatch repair; MSH2, MutS homolog 2; MSH3, MutS homolog 3; MSI1, musashi homolog 1; MUC2, mucin 2; MUFA, monounsaturated fatty acid; NIH, National Institute of Health; NLRP3, NLR family pyrin domain containing 3; NMR, 1H-nucelar magnetic resonance; OA, oelic acids; OLFM4, olfactomedin 4; OXPHOS, oxidative phosphorylation; PA, palmitic acid; PBS, phosphate-buffered saline; PC, phosphatidylcholine; pCEC, primary colonic epithelia cells; PDH, pyruvate dehydrogenase; PE, phosphatidylethanolamine; PGE2, prostaglandin E2; PGE3, prostaglandin E3; PKM, pyruvate kinase isozyme M; PMS2, PMS1 protein homolog 2; PTGER4, prostaglandin E2 receptor 4; PUFA, polyunsaturated fatty acid; PVDF, polyvinylidene fluoride; qISC, quiescent intestinal stem cells; REG4, regenerating family member 4; RN18S, 18S ribosomal ribonucleic acid; RNA, ribonucleic acid; RT-qPCR, quantitative real time polymerase chain reaction; S.D., standard deviation; S.E.M., standard error of the mean SA, stearic acid; SDS-PAGE, sodium dodecyl sulfate-polyacrylamide gel electrophoresis; SFhOGM, serum-free human organoid growth medium; SLC2A1, solute carrier family 2 member 1; SLC2A3, solute carrier family 2 member 3; SLC2A4, solute carrier family 2 member 4; SLC5A1, solute carrier family 5 member 1; SM, sphingomyelin; TA, transient amplifying; TA, transient amplifying; TAG, triacylglycerol; TERT, telomerase reverse transcriptase; TAG, tri(acyl)glyceride; TLR2, toll-like receptor 2; T-TBS, Tween20-Tris-buffered saline; UBC, ubiquitin c; UICC, Union internationale contre le cancer; WD, western-style/westernized diet

*__Correspondence:__

Stefanie Derer

Institute of Nutritional Medicine

University Hospital Schleswig-Holstein, Campus Lübeck

Ratzeburger Allee 160

Tel: +49 451/3101 8402; Fax: +49 451/3101 8404

Stefanie.Derer@uksh.de

ABSTRACT (146 words)

Given the association between early-onset colorectal cancer (eoCRC) and insulin resistance (IR), we investigated the effects of westernized diet (WD)-induced IR on intestinal stem cells (ISCs) by in-depth phenotyping three adolescent mouse models of escalating WD-driven IR. WD-related hyperlipidaemia and hyperglycaemia enhanced ω6-polyunsaturated fatty acid (PUFA) metabolism, while inhibiting glucose metabolism, resulting in colonic epithelial cell (EC) energy deficiency, hypoproliferation, and quiescent ISCs (qISC) expansion. WD-induced systemic IR provoked colonic EC IR, reduced ω6-PUFA metabolism, which was compensated by aberrated triglyceride metabolism and growth factor receptor signalling, causing hyperproliferation of expanded qISCs. Combined with single-cell transcriptomic data and colonic 3D-organoid analysis we revealed that the ω6-PUFA arachidonic acid inhibited glucose uptake, favouring colonic EC IR driven expansion of the lipid-dependent inherently DNA-mismatch prone qISC compartment in expense of the insulin-dependent $LGR5^{+}$ ISCs. Overall, our findings may open new alleys for targeted nutritional interventions in eoCRC prevention.

Introduction

Colorectal cancer (CRC) is the third most common cancer and estimated to reach 3.2 million new global cases in 2040[1]. In recent years, there has been a concerning rise in CRC incidence, particularly among individuals under the age of fifty. Studies, primarily from high-income countries, have reported a marked increase in early-onset colorectal cancer (eoCRC), with the most significant upward trend observed in those under 40 years of age[2–4]. Early adolescence exposure to lifestyle-associated metabolic dysregulation could be a major contributor to eoCRC. Especially westernized, high-calorie, fat-enriched diets strongly promote obesity, insulin resistance and metabolic syndrome (MetS), coupling metabolic-induced chronic inflammation to increased CRC risk[5].

Fatty acids (FAs) are primary constituents of dietary fat and play a critical role as signalling molecules, acting as secondary messengers in physiological regulation and modulating various cellular signalling pathways[6]. Fat-enriched diets include a mixture of FAs from diverse food sources, processed foods, and cultural differences. However, some trends in the types of commonly found FA composition include: monounsaturated FAs (MUFAs; e.g., oleic acid, C18:1), saturated FAs (e.g., palmitic acid, C16:0, and stearic acid, C18:0) and polyunsaturated FAs (PUFAs), commonly ω6 FAs such as linoleic acid (LA, C18:2 ω6), arachidonic acid (AA, C20:4 ω6), as well as ω3 fatty acids (e.g. alpha-linolenic acid, C18:3 ω3). Until a century ago, the dietary ω6 to ω3 ratio was 4:1 or lower. In contrast, the modern Western-style Diet (WD) now features a ratio of approximately 20:1, heavily skewed towards ω6 fatty acids[7,8]. While ω3 PUFAs give rise to anti-inflammatory mediators such as prostaglandin E3 (PGE3), leukotriene B5 (LTB5), and docosahexaenoic acid (DHA), ω6-PUFAs are converted into the pro-inflammatory prostaglandin E2 (PGE2) and leukotriene A4 (LTA4). This imbalance promotes inflammation, as ω6 and ω3 PUFAs compete for the same enzymes, including Δ6/Δ5 desaturases, elongases, cyclooxygenases (COX), and lipoxygenases (ALOX)[9]. Consequently, an ω6-skewed ratio fosters persistent low-grade inflammation[10,11]. Eicosanoid production occurs in distinct phases of tissue repair in a temporally regulated manner. Therefore, if WD-induced damage to colonic tissue combined with excessive intake of ω6-PUFAs leads to a prolonged inflammatory phase and impaired resolution of inflammation, this may result in chronic inflammation and increased tumorigenesis risk[10,12,13]. Notably, elevated levels of AA have been identified in colon cancer tissues, suggesting a pro-proliferative and pro-inflammatory role for AA within the intestinal environment[14].

Intestinal stem cells (ISC) reside at the bottom of the colonic crypt and actively divide to give rise to progenitor cells, which can be categorized into three groups: secretory, absorptive, and stem cell-like progenitors. The secretory and absorptive progenitors proliferate and migrate upward along the crypt, progressively differentiating until they reach the upper crypt region, where they remain before being shed into the lumen[15]. This renewal process takes place every three to five days, is regulated by a variety of differentiation signals and is accompanied by a metabolic switch from glycolysis in ISC to oxidative phosphorylation (OXPHOS) in differentiated cells[16]. The stem cell-like progenitor cell, also called quiescent intestinal stem cell (qISC), remains usually in the +4-position of the colonic crypt and is activated when the active ISC is threatened with damage[17,18]. Further, it has been shown that long-term exposure to a WD markedly reduced the population of active stem cells in the murine colon, while qISC emerged as the principal precursors giving rise to all other colonic cell types[18]. Hence, metabolic environmental changes directly affect the colonic crypt homeostasis, increasing the risk for CRC tumorigenesis[19].

Here, we address the impact of diet-induced colonic epithelial cell (EC) insulin resistance during early adolescence on the colonic crypt homeostasis in mice and its implications on spontaneous colon tumour development.

Results

Constant HFD consumption during adolescence is accompanied by systemic and colonic EC insulin resistance in mice

To determine obesity-related colonic phenotypes after high-fat diet (HFD, **Supplementary Table 1**) consumption during adolescence on the colonic EC compartment, two independent cohorts of 7-week-old mice were fed a high-caloric HFD or a corresponding control diet (CD, **Supplementary Table 1**) for either 6 or 12 weeks. To frame the findings within the context of eoCRC in humans, we calculated the corresponding equivalent human age of the mice using a formula from Wang *et al.*[20] (**Figure 1a**). At the start of the experiment, mice were in early adolescence, corresponding to a human age of 13-14 years. After 6 weeks, they reached late adolescence, equivalent to 21-22 years in humans, and after 12 weeks of intervention, they reached young adulthood, equivalent to a human age of 25 years (**Figure 1a**). As anticipated, HFD-fed mice exhibited significantly greater weight gain compared to their CD littermates in both experiments (**Figure 1b+c**). Furthermore, the 12-week HFD-fed mice displayed significantly greater final weight gain than the 6-week group, resulting in a more pronounced overweight phenotype (**Figure 1d**). After 6 weeks of dietary intervention, a HFD-induced metabolic phenotype was evident in serum 1H-Nuclear Magnetic Resonance (NMR) profiles, as reflected by the distinct clustering of CD- and HFD-derived metabolites in the principal component analysis (**Figure 1e,** a full list of analysed metabolites provided in **Supplementary Table 2**). In detail, acetic acid (p-value= 0.0022, mean-rank diff.= -6.00), lactic acid (p-value= 0.0087, mean-rank diff.= -5.33), and ethanol (p-value= 0.0065, mean-rank diff.= -5.50) were significantly downregulated (**Figure 1f, Supplementary Table 2**). HFD-induced metabolites comprised increased levels of cholesterol (p-value= 0.0022, mean-rank diff.= 6.00) and glucose (p-value= 0.0065, mean-rank diff.= 5.67) (**Figure 1f, Supplementary Table 2**). No differences were detected between both groups regarding analysed amino acids (**Figure 1f, Supplementary Table 2**). After both independent HFD-interventions, mice displayed a significant hyperglycaemic phenotype (median serum D-glucose increase 1.2-fold, 6 weeks; 1.3-fold, 12 weeks), compared to the corresponding CD-fed animals (**Figure 1g**). However, while serum levels of insulin and C-peptide were not altered after 6 weeks of HFD feeding, (**Figure 1h, left panel**), mice exhibited elevated insulin plasma levels as well as systemic insulin resistance after 12-week HFD consumption[21] (**Figure 1h, right panel**). The insulin receptor (INSR) signalling cascade primarily involves the canonical PI3 kinase/AKT pathway, which promotes anabolic processes, such as glucose uptake, protein synthesis, glycogen synthesis,

lipid synthesis, and proliferation[22] (**Figure 1i**). Consistent with the hyperglycaemia observed in HFD-fed mice, colonic *Insr* expression was significantly upregulated after 6 weeks of HFD, whereas a trend towards downregulation was detected after 12 weeks compared to CD controls (**Figure 1j**), indicating the onset of colonic EC-specific insulin resistance at the later time point. Corroborating our results on transcriptional expression after 6 weeks, INSRß levels were significantly elevated, but not in 12-week HFD-fed mice (**Figure 1k**). Of particular note, relative serum glucose concentrations remain comparable between 6 and 12 weeks of HFD, in contrast, colonic INSRβ abundance in colonic tissue of HFD-fed mice is markedly reduced at 12 weeks relative to 6 weeks (**Figure 1g+k**). To functionally study the impact of altered INSR abundance we examined the phosphorylation status of the key downstream mediators AKT and AMPKα to assess alterations in INSR signalling pathway activity. While AKT phosphorylation was not affected, phosphorylation of AMPKα was significantly enhanced in the colonic tissue of 6-week HFD-fed mice (**Figure 1l**), indicating the occurrence of colonic energy deficiency[23]. After 12 weeks of HFD feeding, colonic INSR level were associated with significantly reduced AKT phosphorylation, but no alterations of AMPKα activation (**Figure 1m**). A similar, however more time-dependent decline in AMPKα phosphorylation has previously been reported in a mouse model of HFD-induced insulin resistance, reflecting the opposing roles of AMPKα in energy conservation and AKT in energy-demanding anabolic growth (**Figure 1i**)[24]. In addition to INSR downstream mediators, we assessed expression of key glycolytic enzymes. After 6 weeks of HFD feeding, colonic pyruvate kinase isozymes M (*Pkm*), catalysing the last step of glycolysis by dephosphorylating phosphoenolpyruvate to pyruvate and lactate dehydrogenase A (*Ldha*) were not regulated. The pyruvate dehydrogenase (*Pdh*), catalysing the conversion of pyruvate into acetyl-CoA was not detected in the samples (**Figure 1n**). Notably, decreased serum lactate levels together with hyperglycemia (**Figure 1f+g**) following the 6-week intervention indicate high systemic glucose availability, while intracellular glucose flux might be already limited. Despite the absence of insulin resistance, glucose uptake could be suppressed. Interestingly, Boden *et al.* identified elevated FA availability resulting from HFD as key driver of glucose uptake inhibition[25]. The development of systemic and colonic insulin resistance was associated with decreased colonic *Pkm* and *Pdh* expression, whereas *Ldha* levels remained unaffected (**Figure 1n**), pointing on transcriptional level towards reduced glycolytic flux, which is in line with the detected insulin resistance. Collectively, our results reveal that the 6-week HFD exposure in mice during adolescence disrupts glucose uptake prior to the onset of insulin resistance, whereas the 12-week HFD consumption

induced both systemic and peripheral colonic EC insulin resistance, resulting in an impaired glycolytic flux in colonic ECs.

Young adult mice with colonic EC insulin resistance display an inflamed and hyperproliferative colonic epithelium

Earlier work by Dupaul-Chicoine *et al*. demonstrated that the inflammatory caspase-1 (CASP1) is essential for colonic EC proliferation and tissue repair under inflammatory conditions, thereby playing a pivotal role in preserving intestinal homeostasis[26]. To study the capacity of HFD consumption to trigger intestinal inflammation, caspase-1 was quantified on mRNA and protein levels in colonic tissue. In response to HFD, a significant upregulation of *Casp1* was observed in both interventions (**Figure 2a**). Alongside, a marked increase in CASP1 protein levels was evident after 6 weeks (median 1.53-fold increase), while the same phenotype became more pronounced after 12 weeks of HFD intervention (median 14.75-fold increase) (**Figure 2b**). Remarkably, as indicated by previous findings[21], no macroscopically visible inflammation was detected after 12 weeks of HFD feeding. Complementarily, we recently published that *CASP1* expression positively correlated with *KI67* expression in human CRC tissues[27]. After 6 weeks of HFD feeding, increased CASP1 abundance did not affect *Mki67* expression (**Figure 2c**), while in line with the observed colonic energy deficiency after 6 weeks of HFD, quantification of immunohistochemical staining (IHC) of colonic crypts revealed a significantly decreased abundance of total $Ki67^+$ epithelial cells (**Figure 2d**). In contrast, mice displayed a strongly increased *Mki67* expression after 12 weeks of HFD (**Figure 2e**) which was validated by higher numbers of total $Ki67^+$ epithelial cells in IHC stainings (**Figure 2f**). Hyperproliferation often leads to an elongation of the crypts, as more cells are produced and migrate along the crypt axis[28]. Therefore, colonic crypt length analysis constitutes a standardized marker for the determination of intestinal proliferative activity. Colonic hyperproliferation was accompanied by significantly elongated crypt length in mice after 12 weeks of HFD (HFD median length: 181.000 µm *vs.* CD median length: 156.008 µm, $p = 0.0360$) (**Figure 2g**). This further supports the hypothesis that increased colonic inflammation, in concert with colonic EC insulin resistance, favours CASP1-mediated proliferation of intestinal ECs.

Excessive colonic ω6-PUFA metabolism signalling promotes triglyceride metabolism in WD-related insulin-resistant of mice

Elevated levels of FAs, resulting from diet or derived from bacteria, can activate the NLRP3 inflammasome, resulting in CASP1 activation, and therefore elicit an inflammatory response[26,29,30]. PUFA metabolism in particular has been associated with intestinal inflammation, as excessive dietary intake of PUFAs triggers endoplasmic reticulum stress and activates TLR2 signalling[10]. Further, diet-related luminal FAs have been demonstrated to directly interact with colonic ECs[31]. Hence, we performed a Liquid Chromatography-Mass Spectrometry- (LC/MS) based lipidomic analysis to study the impact of 6-week HFD consumption on faecal lipidome profiles. While 58% of the faecal lipid molecules were significantly upregulated, only 9% lipid molecules were significantly downregulated in HFD-fed mice (**Figure 3a, Supplementary Figure 1a, Supplementary Table 3**). Among the significantly upregulated lipid metabolites, the following candidates displayed high abundances: acylcarnitine (AcCA 18:9; AcCA 24:0), ceramide (Cer d34:0; Cer d34:0; Cer d36:0; Cer d40:0; Cer d36:1), glycosphingolipid (CerG d36:2; CerG d40:0; CerG d40:1; CerG d40:2; CerG 42:2), lysophosphatidylcholine (LPC 16:0; LPC 17:0; LPC 18:0; LPC 20:0; LPC 22:1), phosphatidylcholine (PC 30:0; PC 31:0; PC 32:1; PC 34:1: PC 36:1, PC 36:2; PC 36:4; PC 38:4; PC 38:5; PC 38:6, PC 40:6; PC 40:8), sphingomyelin (SM d32:0; SM d34:0; SM d36:0; SM d36:1; SM d38:0; SM d38:1; SM d39:1; SM d40:0; SM d40:1; SM d41:0; SM d42:0; SM d42:1), and triacylglycerols encompassing mostly saturated or MUFAs (TAG 48:1; TAG 51:1; TAG 52:1; TAG 54:1; TAG 56:0) (**Figure 3a**). Notably, among these upregulated lipid metabolites, free FAs exhibited the greatest upregulation: palmitic acid (PA; C16:0), stearic acid (SA; C18:0), oleic acid (OA; C18:1), arachidic acid (C20:0) and eicosenoic acid (C20:1) (**Figure 3a)**. Additionally, these findings indicate that the colonic epithelium is exposed to excessive FA load, further supporting the hypothesis that glucose uptake is potentially inhibited by FA overload. Most outstanding, the essential ω6-PUFA AA (C20:4) was strongly upregulated in faecal samples from 6-week HFD-fed mice compared to CD-fed mice (**Figure 3a**). Interestingly, AA was recently unravelled to promote intestinal inflammation and inflammation-driven CRC development[10,32,33]. To assess the capacity of FAs to trigger hyperproliferation in the human context, as observed in 12-week HFD-fed mice, the non-cancerous human colonic epithelial cell line HCEC-1CT was cultivated in the presence or absence of HFD-related FAs, including AA, PA, LA, OA, or SA, for five days. Only OA and AA significantly increased HCEC-1CT cell proliferation, with AA stimulation demonstrating the strongest effect (**Figure 3b**). Of note, due to its high

content in the applied HFD, LA (C18:2) was also tested *in vitro*, although it was not upregulated in faecal samples collected from HFD fed mice. However, LA inhibited cell proliferation in HCEC-1CT cells (**Figure 3b**). Furthermore, AA exclusively induced an upregulation of *CASP1* expression (**Figure 3c**) but did not affect *INSR* expression (**Supplementary Figure 1b**). Given that AA uniquely mimics most of the key features of the colonic EC phenotype observed in mice after 12-week HFD-intervention, its mode of action in colonic ECs was further investigated. AA can be metabolized *via* two primary pathways: the cyclooxygenase pathway and the lipoxygenase pathway. COX are the key enzymes in the cyclooxygenase pathway, yielding pro-inflammatory prostaglandins as downstream products, whereas the lipoxygenase pathway is driven by ALOX enzymes, with ALOX5 as the rate-limiting enzyme, leading to leukotriene production[34,35]. Stimulation of HCEC-1CT cells with AA *in vitro* significantly upregulated *COX1* and *COX2*, while *ALOX5* tended to be upregulated (p= 0.095), however, the expression of *ALOX15* was unaffected (**Figure 3d, Supplementary Figure 1c**). Stimulation with PA, SA, or OA did not result in significant changes in the expression of *COX* or *ALOX* enzymes compared to control stimulation (**Supplementary Figure 1d**). However, expression analysis in primary murine colonic epithelial cells (pCECs) revealed *Alox5*, *Alox15*, and diacylglycerol O-acyltransferase 1 (*Dgat1*), a key enzyme in triglyceride (TAG) synthesis and energy storage, to be highly expressed (**Figure 3e**). Whereas *Alox12*, *Cox1*, and *Cox2* were almost undetectable (**Figure 3e**). Based on this basal expression profile, we focused subsequent analyses on the enzymes that were predominantly expressed. After 6-week HFD consumption, only *Alox5* expression was significantly upregulated, while *Alox15*, *Cox1*, and *Cox2*, remained unchanged compared to the CD-fed mice (**Figure 3f+g**, **Supplementary Figure 1e+f).** In contrast, after 12 weeks of HFD consumption, colonic *Alox5* was significantly downregulated, while *Alox15* expression tended to be downregulated compared to CD-fed mice (**Figure 3f+g**), indicative of a switch away from ALOX signalling. On the other hand, expression of enzymes of the COX pathway remained unchanged (**Supplementary Figure 1e+f**). It is known that an excessive amount of exogenous FAs induces DGAT1, which exhibits enhanced TAG biosynthetic activity under HFD conditions[36,37]. Interestingly, stimulation of HCEC-1CT cells with the HFD-related FAs AA, PA, LA, OA, or SA did not alter the expression of *DGAT1* (**Figure 3d, Supplementary Figure 1d**). In the 6-week HFD mouse model, *Dgat1* expression remained unchanged compared to CD-fed controls, which corresponded to unchanged serum TAG levels at this time point (**Figure 3h+i**). In contrast, after 12-week HFD feeding *Dgat1* was significantly upregulated (**Figure 3h**). Intriguingly, serum TAG levels were reduced in HFD compared to CD mice (**Figure 3i**). One possible explanation

is enhanced intracellular diacylglycerol lipase beta (DAGLβ) activity, reflected by the significantly increased colonic *Daglβ* expression (**Figure 3j**), which has recently been reported to exhibit PUFA-specific TAG lipase activity[38]. Additionally, colonic Lipoprotein lipase (*Lpl)* expression was strongly increased in colonic insulin resistant ECs of mice (**Figure 3k**), thereby reflecting accelerated TAG hydrolysis and faster clearance of circulating TAGs, leading to increased FA uptake by colonic ECs. Notably, the high proportion of absorbed FAs may, in part, reflect the hyperproliferative state detected in the insulin resistant mice, which increases a demand for lipids for membrane biosynthesis. In parallel, reduced serum TAG levels and high FA load suggest enhanced intracellular lipid metabolism, which could be reflected by the decreased visceral-to-subcutaneous adipose tissue (vAT/scAT) ratio (**Figure 3l**), as fewer lipids are stored in vAT depots. Increased lipid flux is known to favor mitochondrial FA oxidation[39], suggesting a metabolic switch towards β-oxidation as cellular energy source in the insulin resistant colonic ECs. In the context of CRC progression, a comparison of age-matched healthy colon tissue with paired tumour-adjacent tissue and CRC tissue revealed similarly a significant upregulation of *DGAT1* in both tumour-adjacent and tumour tissue relative to healthy controls (**Figure 3m**). This increased *DGAT1* expression is associated with elevated serum TAG concentrations in CRC patients compared to nonCRC patients (**Figure 3n**), suggesting a role for DGAT1 in the metabolic alterations associated with tumorigenesis. Together, these findings indicate enhanced colonic ω6-PUFA metabolism via ALOX enzymes in mice after 6 weeks of HFD, which becomes attenuated in the colonic EC insulin resistant mice. In compensation, upregulation of colonic *Lpl*, *Dgat1*, and *Daglβ* suggests the establishment of a high-turnover lipid cycle characterized by accelerated FA uptake, transient triglyceride buffering, and remobilization, thereby pointing to high colonic energy supply provided by the excessive FA load.

Excessive colonic ω6-PUFA metabolism inhibits glucose uptake at the expense of LGR5+ ISC proliferation, but drives qISC expansion

As illustrated in the schematic representation of the colonic crypt (**Figure 4a**), its architecture can be divided into four distinct zones: The lower part of the colonic crypt comprises the active cycling stem cell zone, housing cycling, highly glycolytic LGR5^{+}/CD44^{+} ISCs, and REG4^{+}/LYZ^{+} deep secretory cells (DSCs). Adjacent to this, the +4-position harbours the BMI1^{+}/MSI1^{+}/HOPX^{+} qISCs. In a gradual transition, the transient amplifying (TA) zone follows, where HES1^{+}/ATOH1^{+}/SPDEF1^{+} progenitor cells

actively proliferate and migrate upwards within the crypt, towards the mature cell (MC) zone where the fully functional KLF4$^+$/MUC2$^+$ secretory and ALPI$^+$ absorptive cells reside[40]. The cellular composition of the colonic crypt is tightly regulated and shifts in its balance can disrupt crypt homeostasis. To assess whether insulin resistance affects this equilibrium, we analysed the crypt composition in 6-week HFD-fed mice that did not exhibit systemic or colonic insulin resistance. Strikingly, only markers associated with the lower crypt compartment were significantly upregulated in HFD-fed mice compared to CD-fed controls. Specifically, the ISC marker *Lgr5*, the qISC markers *Hopx*, *Bmi1*, and *Msi1*, as well as the DSC marker *Lyz*, showed strong upregulation, while markers of the TA and MC zones were not differentially expressed (**Figure 4b**). To determine whether these alterations persist or evolve with the onset of systemic and colonic EC insulin resistance, we next analysed crypt composition in mice after the 12-week intervention. At the state of colonic EC insulin resistance, increased expression of *Hopx* and *Bmi1* persisted, whereas *Msi1* and *Lgr5* were no longer differentially expressed (**Figure 4c**). Instead, markers for secretory ECs such as *Klf4* or *Reg4* were significantly upregulated (**Figure 4c**). While *Klf4* upregulation implied an involvement in secretory cell differentiation, the absence of increased colonic MUC2 protein levels suggested that the DSC function rather than goblet cell function was expanded (**Figure 4d, Supplementary Figure 1g**). Additionally, analysis of the *CELLxGENE Explorer* dataset "Tabula Muris Senis, Large Intestine - A single-cell transcriptomic atlas characterizing ageing tissues in the mouse (10x)"[41] revealed that elevated *Klf4* expression may also be attributable to *Lyz*$^+$, *Reg4*$^+$, *Bmi1*$^+$, and *Hes1*$^+$ cells, as a notable proportion of these populations co-express *Klf4* (**Supplementary Figure 1h**). Within the TA zone, the absorptive progenitor cell marker *Hes1* was significantly upregulated, while markers of mature absorptive cells were not altered (**Figure 4c**). Taken together, the data mainly point towards an enrichment of qISC and DSCs. Having established the expression profile in murine colonic epithelium after 6- and 12-week intervention, we validated our findings using the non-cancerous HCEC-1CT. Based on established markers for HCEC-1CT cells[42], we unravelled AA to alter the analysed EC marker profile (**Figure 4e**), whereas OA, LA, and SA had no effects (**Supplementary Figure 1i**). In detail, AA treatment led to increased expression of the +4-position marker *BMI1* and significantly decreased expression of the ISC marker *CD44* (**Figure 4e**). Given that HCEC-1CT cells represent a simplified colonic EC model, we extended our analysis to *ex vivo* healthy human colonic 3D-organoids (patient-derived organoids, PDOs), which were stimulated with AA or control for a 10-day period. AA exposure enhanced organoid growth, with significantly increased growth from day 3 onwards (**Figure 4f**). Moreover, AA stimulation induced a morphological shift, with organoids transitioning from

the typical budding morphology towards a more spheroid-like structure (**Figure 4g**). These morphological changes are an indication of an altered cellular composition and metabolic shifts, as organoid architecture can be linked to both stem cell abundance and epithelial integrity[43,44]. We therefore examined whether AA stimulation affected organoid cell composition and metabolism. AA stimulation had effects on the +4-position and mature secretory cell populations of the colonic organoids, which reflects the findings from the mouse models (**Figure 4h**). Of note, a recent study demonstrated that AA activates WNT signalling, possibly stimulating +4-position cells in an $LGR5^{+}$-independent manner[45]. Compared to controls, the +4-position markers *BMI1* (median 1.3-fold), secretory lineage markers such as *MUC2* (median 9.24-fold), *KLF4* (median 1.5-fold), *LYZ* (median 2.0-fold), EGF (median 1.7-fold) or *REG4* (median 4.0-fold), along with the enterocyte marker *ALPI* (median 1.9-fold) were significantly increased (**Figure 4h**). Furthermore, analysis of the supernatant of AA-stimulated human organoids between days 8 to 10 revealed strong ω6-PUFA metabolism reflected by increased PGE_2 secretion (**Figure 4i**). Of note, increased PGE_2 is associated with chronic low-grade inflammation[46]. However, the expression of *CASP1* was not significantly altered by AA compared to control (**Supplementary Figure 1j**). Additionally, elevated PGE_2 secretion suggests the contribution of COX enzymes in the metabolism of AA in human colonic ECs. Although, AA stimulation did not alter *COX1/2* expression, elevated PGE_2 secretion may indicate enhanced COX activity (**Figure 4j**). Notably, increased activity of prostaglandin E synthases may also underlie this effect[47]. Furthermore, *ALOX5* and *DGAT1* were upregulated by AA stimulation *(***Figure 4j***).* Interestingly*,* the main enzyme for cholesterol production *HMGCS1* was significantly downregulated (**Figure 4j**). This cloud align with DGAT's role in promoting cholesterol uptake, which reduces the need for endogenous cholesterol production[48]. The supernatant of AA-stimulated organoids contained significantly lower concentration of glycerides, including mono-, di- and triglycerides (**Figure 4k**). Consistent with the findings in the mouse model, our data suggest that upstream of Dgat1, glycerol-3-phosphate availability might be limited due to reduced glycolytic activity, while fatty acids are preferentially directed toward β-oxidation. This is supported by the decreased glucose consumption observed in four of five stimulated PDOs (**Figure 4l**), pointing towards decreased or inhibited glucose uptake. Additionally, within the glucose metabolism pathway, *INSR* expression was significantly upregulated in colonic PDOs stimulated with AA (**Figure 4m**). However, neither the insulin-dependent glucose transporter *SLC2A4* nor the insulin-independent *SLC2A1* was differentially expressed (**Figure 4m**). Moreover glucose transporter *SLC2A3* was significantly downregulated (**Figure 4m**). Instead, the sodium-dependent transporter *SLC5A1* showed a strong trend towards upregulation

and likely compensates for impaired insulin-dependent glucose uptake (**Figure 4m**). Additionally, unchanged *LDHA* expression may point to a shift towards aerobic glycolytic flux (**Figure 4m**). Despite increased *INSR* expression, insulin consumption by AA-stimulated organoids was significantly decreased compared to control (**Figure 4n**). Together, excessive colonic ω6-PUFA metabolism in insulin sensitive colonic ECs, as observed in 6-week HFD-fed mice, boosted the qISC and DSC compartments. In contrast, reduced ω6-PUFA metabolism in insulin resistant colonic ECs, as observed in 12-week HFD-fed mice, suppressed the $LGR5^+$ stem cell pool while promoting expansion of TA cells, qISC and DSC populations. Furthermore, excessive extracellular AA load is highly likely to contribute to impaired glucose uptake and thereby long-term to reduce insulin-sensitivity in a long-term perspective.

Proliferation of $LGR5^+$ ISC is driven by INSR signalling, while qISC proliferation depends on growth factor receptor and lipid signalling

To further exacerbate the observed insulin-resistant phenotype and to assess the impact on colonic ECs, mice were subjected to a prolonged western-style diet (WD; **Supplementary Table 1**) for 24 weeks. The utilized model is considered a gold standard for inducing MetS in rodents, as its combination of high-fat content and added fructose and sucrose promotes lipogenesis, elevates plasma insulin, leptin, TAG, glucose, and free FAs, and simultaneously impairs glucose tolerance[49,50]. WD-fed mice exhibited significantly reduced colonic expression of *Lgr5* and *Insr*, while expression of the qISC markers *Bmi1* and *Tert* were increased compared to CD-fed controls (**Figure 5a+b**). The diminished *Insr* expression was reflected by significantly reduced colonic protein abundance in WD-fed mice (**Figure 5c, Supplementary Figure 1k**). Consistent with the 12-week HFD intervention, a colonic EC insulin resistance was established as indicated by reduced INSR downstream AKT phosphorylation (**Figure 5d, Supplementary Figure 1l**). Here, activation of colonic AMPKα remains unaffected (**Figure 5d, Supplementary Figure 1l**), suggesting preserved cellular energy availability in colonic tissue despite insulin resistance. Complementing the decreased *Lgr5* expression and reduced INSR-signalling in the colonic tissue, corresponding WD-derived colonic organoids exhibited significantly reduced growth from day 7 onward under WNT-dependent culture conditions, remaining smaller and exhibiting less pronounced crypt-like structures compared to colonic organoids derived from CD-fed controls (**Figure 5e+f, Supplementary Figure 2a**). Notably, *Insr* downregulation in WD colonic tissue was preserved in the corresponding organoids compared to CD-derived organoids (**Figure 5g**). As stem cells

predominantly rely on glycolysis for energy production[51] and have high proliferative capacity, insulin signalling is critical for nutrient uptake, such as glucose, FAs or amino acids. Our findings from the two independent mouse models of systemic insulin resistance, including the 12-week HFD and 24-week WD, demonstrate the development of colonic EC insulin resistance and thereby disruption of the self-renewal capacity of the LGR5$^+$ ISCs. To further elucidate the contribution of INSR to colonic crypt homeostasis, we interrogated single-cell transcriptomic data from healthy adults' large intestine and rectum by using the *CELLxGENE Explorer*[41], revealing that *INSR* expressing cells (*INSR*$^+$) closely overlapped with *CTNNB1*$^+$ cells (**Figure 5h**). Additionally, we identified two distinct populations within *CTNNB1*$^+$ cells marked by highest INSR expression (**Figure 5h**). Given that *CTNNB1* encodes β-catenin, a central effector of canonical WNT signalling, which governs the balance between LGR5$^+$ ISC maintenance, proliferation, and differentiation[52], we hypothesized that especially cells of the lower crypt rely on INSR signalling for proliferation. Using cell annotation *via CELLxGENE Explorer*, we confirmed that cells exhibiting elevated INSR and CTNNB1 expression reside primarily within ISC and the TA zone, while low expression was found in absorptive colonocytes (**Figure 5h**). Furthermore, there is evidence that INSR signalling has the ability to activate the β-catenin pathway[53]. Complementing, nearly all *INSR*$^+$ colonic ECs also express *CTNNB1*, accounting for approximately one quarter of the total *CTNNB1*$^+$ cell population (**Figure 5h**). In the next step, we analysed which cell types within the lower crypt co-express *CTNNB1* and *INSR*, focusing on markers for EC subpopulations that were mainly affected by the presence of colonic insulin resistance such as ISC and qISC, but also DSCs, as these cells provide the niche for ISC[54]. Across all markers, approximately one quarter of the respective marker-positive cells co-express *CTNNB1* and *INSR* (**Figure 5i**). To characterize molecular expressional differences underlying the two *CTNNB1*$^+$*INSR*$^{+high}$ clusters with the highest expression levels, differential gene expression analysis was performed using *CELLxGENE Explorer*. Amongst other markers the upper *CTNNB1*$^+$*INSR*$^{+high}$ cluster was strongly enriched for *RARRES2*$^+$ cells. Notably, RARRES2 has been reported to be highly abundant in ISC, but is also found to a much lesser extend in secretory progenitor cells[55]. In contrast, the lower *CTNNB1*$^+$*INSR*$^{+high}$ cluster was characterized by enrichment of OLFM4$^+$ cells, a marker associated with absorptive ECs in the colon[55]. Furthermore, established markers of active and quiescent colonic ISC populations, including *LGR5*, *ASCL2*, *CD44*, *BMI1*, *LRIG1*, *LGR4*, and *MSI1*, were predominantly localized within *CTNNB1*$^+$*INSR*$^{+high}$ cell populations. In addition, markers of DSCs, such as *LYZ* and *REG4*, were also predominantly enriched in the *CTNNB1*$^+$*INSR*$^{+high}$ populations. No specific enrichment within the *CTNNB1*$^+$*INSR*$^+$ cluster was observed for *HOPX*, but the number of

cells positive for *CTNNB1*$^{+}$*INSR*$^{+}$*HOPX*$^{+}$ was strongly limited (**Figure 5j**). Although qISCs contain a similar number of *INSR*$^{+}$ cells as active *LGR5*$^{+}$ ISCs, they appear better equipped to withstand insulin resistance, potentially due to higher expression of other growth factor receptors (**Figure 5k**). Specifically, *CTNNB1*$^{+}$*INSR*$^{+}$ qISCs exhibited elevated expression of FA and lipid-associated receptors, including *PTGER4*, *APOBR*, and *LDLR*, relative to ISC populations (**Figure 5k**), suggesting that these cells may strongly respond to lipid-mediated signalling, as detected in HFD-fed mice. Additionally, higher levels of receptor tyrosine kinases such as growth factor receptors *ERBBR2/3*$^{+}$, *EGFR*$^{+}$ and *IGF2R*$^{+}$ were detected for *CTNNB1*$^{+}$*INSR*$^{+}$ qISCs compared to LGR5^{+} ISCs (**Figure 5k**). Particularly, *CTNNB1*$^{+}$*INSR*$^{+}$*RARRES*$^{+}$ cells exhibit extremely low expression of lipid and growth factor receptors, underlining the pivotal role of INSR signalling in this ISC population. Consistent with the findings from *CELLxGENE Explorer* single-cell transcriptomic dataset, we identified elevated activation of the MAPK p44/42, a downstream effector of the receptor tyrosine kinases, in the mouse models of 12- or 24-week diet-induced insulin resistance (**Figure 5l**). Notably, *CTNNB1*$^{+}$*INSR*$^{+}$ qISCs display higher *TNFRSF1A* and *IL6R* expression than ISCs, with *CTNNB1*$^{+}$*INSR*$^{+}$*HOPX*$^{+}$ qISCs expressing highest *IL6R* levels. High activation of *TNFRSF1A* and *IL6R* could downstream result in elevated MAPK p44/42 activation and hence proliferation under inflammatory conditions. Supporting this, Nickel *et al.* demonstrated that IL-6, a key marker of chronic inflammation, was elevated in mice after 12-week HFD[21]. Consistently, colonic *Hopx* expression was significantly increased in both independent models of HFD feeding (**Figure 4c**). Our findings suggest that under conditions of diet-induced excessive colonic ω6-PUFA metabolism and insulin resistance, qISCs possess a broader repertoire of growth factor receptors, which cloud drive unbalanced hyperproliferation of this population.

Colonic expansion of inherently DNA error-prone qISC is associated with downregulation of MSH2

Previous findings by Li *et al.* demonstrated interference of diet with DNA-repair mechanisms[18] . Our data revealed that HFD-associated colonic EC insulin resistance promotes inflammation-driven hyperproliferation and expansion of inherently more DNA mismatch-prone qISC[56]. Hence, we hypothesized that increased DNA replication rates due to hyperproliferation may contribute to a higher risk of DNA damage accumulation, thereby potentially acting as an initiator of tumorigenesis. A primary system responsible for maintaining genomic integrity is the DNA mismatch repair (MMR) system. Here,

MutS homolog 2 (MSH2) forms heterodimers with MSH3 or MSH6, these heterodimers associate with MutL homolog 1 (MLH1) and PMS1 protein homolog 2 (PMS2) to form a functional MMR complex (**Figure 6a**). First, we investigated colonic MMR enzyme expression in CD-fed mice. *Msh2* displayed the highest expression in the colonic compartment compared to *Mlh1* and *Pms2* (**Figure 6b**), underlining the pivotal role of MSH2 in the initiation of the MMR complex. Protein analysis revealed a significantly higher abundance of MSH2 in insulin-sensitive colonic tissue (6 weeks of HFD), whereas a significant downregulation was observed in insulin-resistant colonic tissue (**Figure 6c**). Further analyses identified colonic MSH2 protein level to correlate with total body weight of the mice after the 6-week intervention, while it was negatively correlated with body weight in mice with colonic EC insulin resistance (**Figure 6d**). To assess whether HFD-associated FAs contribute to the downregulation of MSH2, we evaluated their effects *in vitro*. Among the tested FAs, AA and PA significantly reduced MSH2 expression in HCEC-1CT cells compared control (**Figure 6e, Supplementary Figure 1m**). To translate the findings from the mouse study in the context of CRC, we investigated the baseline state of the MMR complex enzymes in human colon biopsies. In healthy age-matched colonic tissue from hospitalized individuals (nonCRC), level of *MSH2* and *MLH1* were comparable, whereas *PMS2* expression was significantly lower than that of the aforementioned (**Figure 6f**). Notably, *MSH2* expression was significantly lower in normal colonic tissue adjacent to the tumour site compared to paired tumour tissue from patients with CRC and nonCRC tissue, while no differences were detected between the latter two (**Figure 6g**). To gain deeper insights into the basal expression of *MSH2* at different tumour stages, paired samples of adjacent normal tissue and tumour tissue were sorted by tumour stage, based on *Union internationale contre le cancer* (UICC) classification. We found that adjacent normal tissue showed significantly reduced *MSH2* exclusively in stage I, while only a non-significant trend towards decreased expression was detected between adjacent normal and tumour tissues in stages II-IV (**Figure 6h**). Further, the data demonstrated a significant downregulation of *MSH2* in tumour tissue among the UICC stages II and III+IV in comparison to stage I (**Figure 6h**). In summary, colonic level of MMR and especially MSH2 were downregulated in a body-weight-dependent manner in 12-week HFD-fed mice that display colonic EC insulin resistance and hyperproliferation. Furthermore, *MSH2* was reduced in the colonic tissue with a higher cancer susceptibility (adjacent tissue), potentially contributing to impaired DNA repair capacity. Together, the data suggest that with advancing tumour progression, the MMR system becomes progressively suppressed, primarily through the downregulation of MSH2.

Discussion

The environmental risk factors of sporadic eoCRC remain poorly defined. Over recent decades, profound lifestyle and behavioural changes have been proposed to contribute to the decreasing age of CRC onset[57–60]. Among the various lifestyle factors implicated in eoCRC, diet is increasingly recognized as one of the most decisive contributors. In the present study, we address the impact of diet-induced colonic ECs insulin resistance during early adolescence on the colonic crypt homeostasis in mice and its implications on human colonic EC homeostasis. Therefore, colonic ECs of three independent adolescent mouse models of progressive WD-driven insulin resistance were phenotyped in-depth.

We demonstrated that HFD not only induced a systemic insulin resistance, as previously reported[21,49,50], but also elicited colonic EC-specific insulin resistance. This was observed in 12-week HFD-fed mice showing clear signs of impaired insulin receptor signalling in the colonic epithelium. Faecal lipidomic profiling of late adolescent mice after 6 weeks of HFD identified the HFD-associated PUFA AA, which was further found to inhibit glucose uptake in insulin-sensitive colonic ECs. Further, this inhibition links to sustained upregulation of INSR, a phenomenon recapitulated in both 6-week HFD-fed mice and healthy *ex vivo* human colonic organoids treated with AA. Chronic INSR overexpression and hyperactivation can trigger receptor internalization, activate negative feedback mechanisms that dampen downstream signalling. Furthermore, after 6 weeks of HFD, FAs are preferentially metabolized by ALOX and COX pathways and lipid accumulation in the form of stored in visceral and subcutaneous adipose tissue, resulting in colonic EC energy deficiency and hypoproliferation. Ultimately, this culminates in an adaptive desensitization of insulin signalling, functioning as a protective mechanism against chronic overstimulation, but manifesting as insulin resistance[61]. Insulin-resistant colonic EC metabolism shifts from ALOX signalling towards energy production via β-oxidation and likely provision of FAs for membrane synthesis to support hyperproliferation. Concurrently, greater lipid uptake by tissues leads to a reduction in serum TAG levels. Notably, less visceral fat accumulates relative to subcutaneous fat, supporting the hypothesis of increased intracellular lipid consumption.

Our study demonstrates that colonic EC-specific insulin resistance can arise alongside systemic resistance or may be driven by hyperglycaemia and hyperlipidaemia. As colonic ECs are continuously exposed to high basolateral glucose, overstimulation of the colonic EC INSR may lead to diminished insulin signalling. Notably, mice exhibiting systemic insulin resistance after 12 weeks of HFD showed unchanged colonic INSR abundance despite hyperglycaemia. Nevertheless, INSR downstream kinase

AKT was significantly less activated, as well as main glycolytic enzymes, overall indicating colonic EC-specific insulin resistance. This state was accompanied by colonic EC hyperproliferation, inflammation, and aberrant TAG metabolism. Ostermann and colleagues similarly observed reduced AKT phosphorylation in the colonic tissue of obese mice[62].

Based on the reduced growth capacity of our organoids derived from insulin-resistant WD-fed mice, colonic EC insulin resistance likely imposes a metabolic constraint on the epithelium. In particular, glucose-dependent self-renewal of active ISC was impaired, as these cells rely heavily on glycolysis and glucose uptake to support their proliferative activity[51,63]. While we showed reduced growth capacity of organoids derived from WD-fed mice, Ostermann *et al*. showed a decreased seeding capacity of organoids derived from insulin-resistant mice[62], and Andres and colleagues demonstrated that a specific deletion of the INSR in small intestinal epithelial tissue led to a decrease in the expression of stem cell markers[64], all highlighting the important role of the INSR in the stem cell compartment. However, upon HFD-feeding of intestinal EC-specific INSR deficient mice Andres *et al.* showed reduced expression of qISC markers *Bmi1*, *Lrig1*, and *Hopx*[64]. Importantly, that study examined the small intestine, whereas our analyses focused on colonic tissue, which may account for the different findings regarding the qISC expression profile.

A recent study demonstrated that loss of *Insr* expression potentiated intestinal inflammation and impaired mucosal healing following AOM/DSS challenge in mice[62]. We demonstrated that AA-driven metabolic impairment of ISCs may compromise colonic homeostasis, the maintained regenerative capacity suggests compensatory activation of an alternative stem cell-like population for mucosal repair. Previously it has been described that, qISC can smoothly transition to maintaining mucosal homeostasis when the active ISCs are ablated or threatened by damage due to radiation or environmental factors[65]. A similar effect was found by Wang *et al*., who were able to identify an increase in qISC and enhanced proliferation rates by stimulating mouse small intestinal organoids with AA[45]. Our data indicate that qISCs express higher levels of INSR-independent growth factor receptors (especially *EGFR* and *ERBB2/3)*, might display higher responsiveness to inflammation-driven IL-6 signalling due to greater *IL6R* expression, and likely possess a greater repertoire of ω6-PUFA-dependent and other lipid receptors. This combination renders qISCs not only more insulin-independent than active ISCs but also more prone to proliferation under pro-inflammatory conditions associated with high lipid accumulation or colonic EC-specific insulin resistance. Additionally, the murine small-intestinal organoids used in the

study by Wang *et al*. displayed morphological alterations[45], which appeared similar to those observed in our work. The spheroid-like phenotype may be a result of the presence of PGE_2, which accumulates in the medium of AA-stimulated organoids as a product of AA metabolism and might also be a potent driver of cellular compositional changes. Furthermore, it has been shown that PGE_2 induces proliferation and may also contribute to ion channel activation[45,66,67]. It is important to emphasize that the experiments in this study were conducted under conditions of excess AA to colonic ECs. Under balanced conditions, downstream metabolites of AA have been implicated in tissue repair and the resolution of inflammation[12]. This suggests that AA signalling follows a beneficial balance under normal healthy physiological conditions, whereas disruption of this equilibrium by excessive dietary AA intake may compromise intestinal homeostasis.

The qISC population plays a protective role by safeguarding homeostatic ISCs and maintaining tissue integrity under AA-driven inflammation. However, long-term activation of qISCs may increase mutation burden, as these cells exhibit inherently higher error rates, because of reduced efficiency in DNA MMR[17]. Consistently, we observed a reduction in MSH2, a key MMR enzyme, in the 12-week HFD-mice, despite hyperproliferation. Supporting this, Li *et al.* demonstrated that under a NWD1 diet, increased contribution of the $BMI1^+$ qISCs to mucosal maintenance is associated with a higher mutation load[18]. Thus, both the elevated mutation burden and the stem/progenitor potential of $BMI1^+$ cells may enhance the tumorigenic potential[19,68]. While Li and colleagues attributed these effects primarily to dietary vitamin D deficiency, our data suggests that excessive levels of the WD-associated AA can similarly promote qISC activation and might also be associated with a higher mutagenic risk.

In conclusion, exposure to a WD primes colonic EC, promoting metabolic colonic EC insulin resistance and therefore may increase susceptibility to neoplastic transformation of colonic ECs. Our findings indicate that this effect is associated with activation of the inherently DNA mismatch-prone qISC population, which compensates to maintain intestinal homeostasis under metabolic stress[18,19]. These findings may have translational relevance, as a WD could trigger comparable early cellular alterations in younger human individuals, persisting over time and thereby contributing to the rising incidence of eoCRC. Importantly, early detection of colonic EC insulin resistance may open opportunities for targeted nutritional interventions to mitigate the elevated CRC risk in this population.

Methods

Patient Recruitment and Sample Collection

RNA from CRC patients utilized for quantitative real time PCR (RT-qPCR) was purchased from OriGene (OriGene Technologies, Inc., Rockville, MD, USA).

Colonic biopsies from healthy individuals were obtained during endoscopy as part of regular patient management in the Medical Department 1, University Hospital Schleswig-Holstein Campus Lübeck, Germany. Biopsy specimens were obtained from descending colon, sigmoid colon, and rectum. Serum samples of healthy fasted patients (nonCRC) were collected during routine patient management in the Medical Department 1, University Hospital Schleswig-Holstein Campus Lübeck, Germany. Serum samples of patients with CRC were collected prior to administering anaesthesia during surgery. All patients gave written informed consent for sample donation and protocols were approved by the ethics committee of the University of Lübeck (Az-21-415; Az-16-282; Az-05-112). Patients' characteristics are depicted in **Supplementary Table 4**.

Animal experiments

The 6-week HFD intervention experiment was conducted at Cincinnati Children's Hospital Medical Center (CCHMC), United States and approved by the CCHMC Animal Care and Use Committee (Animal proposal number: IACUC2020-0034). The other animal experiments were approved by the Ministry of Energy, Agriculture, the Environment, Nature and Digitalization Schleswig-Holstein, Germany (12-week HFD intervention: 242-50006/2016(109-8/15); 24-week dietary intervention: 242-46069/2022(47-6/22)). All animal care and experimental procedures were performed in accordance with the National Institutes of Health (NIH) guidelines and in accordance with Animal Research: Reporting of In Vivo Experiments (ARRIVE) guidelines. All mice were housed under specific pathogen-free conditions on a regular 12-hour light-dark cycle with *ad libitum* access to food (specified in **Supplementary Table 1**) and water.

For the 6-week HFD intervention, male C57BL/6J mice (Jackson Laboratories, ME, USA) were habituated to laboratory conditions for at least 10 days prior to the start of the experiment. Mice were randomly assigned either a control diet (CD, Autoclavable rodent diet 5010, LabDiet, St. Louis, USA) or

the HFD D12492i (Research Diets Inc., New Brunswick, USA). All mice were sacrificed at the end of the 6th week for serum and organ collection.

For the 12-week HFD feeding model, male C57BL/6N mice (Charles River Laboratories, Sulzfeld, Germany) were used, receiving either a regular chow diet (CD, EF acc. D12450B mod., ssniff®, Soest, Germany) with vehicle treatment or HFD (EF acc. D12492 [I] mod., ssniff®, Soest, Germany) with vehicle treatment, as previously described [21].

For murine colonic organoid generation, male mice were ordered from University Medical Center of Johannes Gutenberg University Mainz (Mainz, Germany). The Dnmt1 2lox mice were made as a congenic strain by backcrossing to C57BL/6 for 10 generations and then intercrossing to homozygous the 2lox allele (JAX Lab, Dnmt1 flx/flx). Embryos of these mice were transferred and bred in the animal facility of the University of Lübeck. Male Dnmt1 flx/flx mice, corresponding to wildtype C57BL/6 were randomly assigned into two groups placed on the Control (to Surwit) diet (ssniff®, Soest, Germany) starting at 4 to 6 weeks of age. After 2 weeks on the Control (to Surwit) diet, animals were randomly assigned to two groups: one group remained on the Control (to Surwit) diet, while the other was switched to the Surwit diet supplemented with sucrose (EF acc. D12331, ssniff®, Soest, Germany) and supplemented with 45% (w/v) glucose and 55% (w/v) fructose *via* the drinking water. Mice were maintained on the respective diet for 24 weeks (median age 222 days, IQR 215-226.5 days) before organ sampling.

Generation of murine and human colonic 3D-organoids

Human and murine colonic crypts were isolated using protocols from StemCell™ Technologies. Briefly, colon from WD- and CD-fed mice were washed in cold DPBS (Gibco, Waltham, MA, USA, #14190144) and incubated with Gentle Cell Dissociation Reagent (GCDR; StemCell™ Technologies, Vancouver, Canada, #100-0485) for 45 minutes at room temperature. Supernatants were passed through 70 µm filters (StemCell™ Technologies), and fractions enriched in crypts were collected, centrifuged, and resuspended in cold DMEM/F12 (Gibco, #11530566). After a second centrifugation, crypts were embedded in UltiMatrix Reduced Growth Factor Basement Membrane Extract (UltiMatrix; R&D Systems, Minneapolis, USA, #BME001) and seeded in 50 µL domes in pre-warmed 24-well plates (Sarstedt, Nürnbrecht, Germany, #83.3922.300). Domes were solidified at 37°C for 30 minutes, overlaid

with IntestiCult™ Organoid Growth Medium (StemCell™ Technologies, #06010) supplemented with 100 ng/µl IGF1 (PeproTech Gmbh, Hamburg, Germany, #250-90), and 50 ng/µl FGF-basic (PeproTech Gmbh, Hamburg, Germany, #450-33), and maintained at 37°C, 5% CO_2, with medium changes every 2-3 days.

Human colonic crypts were obtained from biopsy specimens of the descending colon, sigmoid colon, and rectum. Samples were washed, minced, and incubated in GCDR (StemCell™ Technologies). After centrifugation, fragments were resuspended in cold DMEM/F12 (Gibco) supplemented with 1% (w/v) BSA (AppliChem/Illinois Tool Works Inc., Chicago, USA, #A1391) and 15 mM HEPES (Gibco, #15630-056). Supernatants were filtered, crypts counted, quality assessed and then pelleted. Isolated crypts were mixed 1:1 (v/v) with Human IntestiCult™ Serum-free Organoid Growth Medium (SFhOGM; StemCell™ Technologies, #100-0340) and Cultrex BME Type 2 (Cultrex; R&D Systems, #3533). Approximately 1000 crypts per 50 µL dome were seeded to a 24-well plate (Sarstedt) and maintained at 37°C, 5% CO_2, with medium changes every 2-3 days.

Generation of murine primary colonic epithelial cells (pCEC)

The colon of sacrificed mice was excised, opened longitudinally, washed, and cut into small pieces. Tissue fragments were shaken for 10 minutes in 1 mM dithiothreitol (DTT, Carl Roth, Karlsruhe, Germany, #6908) in PBS (Gibco) at room temperature. After removing the supernatant, the pieces were incubated for 2 hours in 1 U/ml Dispase (StemCell™ Technologies) in PBS (Gibco) containing 1% (w/v) BSA (AppliChem/Illinois Tool Works Inc.) at 37°C with agitation. The resulting suspension was passed through a 70 µm cell strainer (Sarstedt), washed with PBS, isolated cells were subsequently counted and further processed.

Organoid culture

Primary organoid cultures were passaged after 7 to 14 days. Medium was removed, and cold GCDR was added to the dome. After one minute incubation with GCDR at room temperature, the dome and organoids were disrupted by pipetting the suspension. The well was washed again with GCDR. After incubating the organoids on ice for 10 minutes, followed by centrifugation, organoids were washed in

DMEM/F12 with 15mM HEPES containing 1% (w/v) BSA, centrifuged and resuspended in a 1:1 (v/v) mixture of SFhOGM (StemCell™ Technologies) and Cultrex (R&D Systems) or pure UltiMatrix (R&D Systems), respectively. Next, 50 µl domes were formed on a 24-well plate (Sarstedt) and placed at 37°C for solidification. The domes containing human colonic organoids were overlaid with 500 µl SFhOGM and domes containing murine colonic organoids were overlaid with 500 µl IntestiCult™ Organoid Growth Medium supplemented with 100 ng/µl IGF1 (Pepro Tech Gmbh) and 50 ng/µl FGF-basic (Pepro Tech Gmbh). Complete medium changes were performed every 2-3 days.

Real-time proliferation analysis of 3D-organoid culture

Real-time proliferation data were obtained using the IncuCyte SX5 (Sartorius, Göttingen, Germany). Organoids were seeded into a 48-well plate (Corning, Glandale, USA, #CLS3548) according to the protocols provided by Sartorius. For stimulation 10 µM arachidonic acid (AA; Sigma Aldrich, MO, USA #10931), dissolved in DMSO, or a respective DMSO control (containing ≤ 0.1% DMSO, Sigma Aldrich, #D2438) were freshly added to the medium. Every 48 hours, organoid culture medium was renewed containing respective stimuli. Continuous growth of organoids was quantified every 6 hours for a total of 10 days using the IncuCyte Imaging System (Essen BioScience, Ann Arbor, USA). The average Organoid Object Total Brightfield Area ($*10^4$) in μm^2 was normalized to 0 days 0 hours 0 minutes. Analysis was conducted using IncuCyte Organoid QC analysis software (v2022B Rev2, Satorius).

Cell culture

Immortalized human colonic epithelial cell line HCEC-1CT was kindly provided by Damian Graczyk (Institute of Biochemistry and Biophysics Polish Academy of Sciences, Warsaw, Poland) with permission from Jerry W. Shay (UT Southwestern Medical Center, TX, USA). The cells were grown in DMEM/F12 (1:1) (Gibco) containing 2% (v/v) heat-inactivated fetal calf serum (FCS), 100 U/ml penicillin, and 100 mg/ml streptomycin. With each passage the medium was freshly supplemented with 1 µg/ml hydrocortisone (Sigma Aldrich, #I0516), 5 nM sodium selenite (ThermoFisher Scientific, Waltham, USA, #11366449), 20 ng/ml recombinant human epidermal growth factor (EGF; Roche, Basel, Swizerland, #11376454001), 10 µg/ml insulin (Sigma Aldrich,), and 2 µg/ml human holo-transferrin (Biozol, Echingen, Germany, #ABM-G599). For fatty acid (FA) stimulation, 50,000 cells/well were seeded into a

24-well plate. After 24 hours, 10 µM AA (Sigma-Aldrich) or palmitic acid (PA; Sigma-Aldrich, #P0500) dissolved in DMSO, linoleic acid (LA; Sigma-Aldrich, # L5900) or oleic acid (OA; Sigma-Aldrich, #O1257) dissolved in DEPC-treated water (Gibco), or 10 µM stearic acid (SA; Sigma-Aldrich, #800673) dissolved in absolute ethanol (EtOH; Carl Roth, 5054) were added to each well. Medium and FA stimulation were refreshed after 96 hours, and cells were harvested after 144 hours (6 days) for counting using the QuadCount™ (Accuris Instruments, Sayreville, USA) and subsequent analyses.

RNA extraction, cDNA synthesis and quantitative real-time PCR

Isolation of total RNA from HCEC-1CT cells, human colonic biopsies or murine colonic tissues was performed using the innuPREP RNA Mini Kit (Analytic Jena AG, Jena, Germany, #845-KS-2040010) according to the manufacturer's instructions. Isolation of total RNA from organoids was performed using the Norgen Single Cell Isolation Kit (Norgen Biotek Corp., Thorold, Canada, #SKU51800) according to the manufacturer's instructions. After binding of RNA to the RNA column, additional DNA digestion was performed with 4 units of DNase I (Sigma Aldrich, #AMPD1-1KT). RNA quality was assessed using the Agilent 2100 Bioanalyzer (Agilent Technologies, CA, USA), and samples with a RIN ≤ 3.0 were excluded.

For cDNA synthesis, a maximum of 1 µg RNA was transcribed utilizing Oligo(dT)18 primers and the RevertAid H Minus reverse transcriptase (Thermo Fisher Scientific #EP0451).

Target amplification was performed by RT-qPCR on the StepOnePlus™ or the QuantStudio™ 1 system (Thermo Fisher Scientific), in combination with the PerfeCTaTM SYBR® Green SuperMix (Quantabio, MA, USA, #95055-02K) and target-specific oligonucleotides (listed in **Supplementary Table 5**). Data were analysed using the $2^{-\Delta CT}$ or $2^{-\Delta\Delta CT}$ algorithm (for murine colonic samples to the median CD target expression for each of the respective animal experiments, due to baseline variations) by normalization to *Actb, ACTB*, *Ubc*, *UBC*, or *Rn18S*.

Protein isolation from formalin-fixed paraffin-embedded (FFPE) tissue

To isolate proteins from FFPE colon tissue, the Qproteom FFPE Kit from Qiagen (QIAGEN N.V., Venlo, Netherlands, #37502) was used according to manufacturer's instructions. Whole protein concentration was determined using the Roti® Quant universal assay (Carl Roth, #0120).

Sodium Dodecyl Sulfate-Polyacrylamide Gel Electrophoresis (SDS-PAGE) and Immunoblotting

For SDS-PAGE, whole protein extracts were separated on a CriterionTM TGXTM 4-15% polyacrylamide gel (Bio-Rad, CA, USA, #5671085). Separated proteins were blotted to a PVDF membrane by semi-dry transfer. After blocking in 5% (w/v) non-fat milk in Tween20-Tris-buffered saline (T-TBS), membranes were probed with specific primary antibodies (**Supplementary Table 6**), followed by respective horseradish peroxidase (HRP)-conjugated secondary antibodies. Specific proteins were detected using chemiluminescent HRP substrate on the ChemiDocTM XRS+ (Bio-Rad) or the iBright 1500 imaging system (ThermoFisher) and quantified in ImageJ. To ensure similar transfer and equal loading of proteins, the abundance of target proteins was normalized to α-Tubulin.

Dot blot

Protein samples were directly applied onto nitrocellulose membranes (Amersham™ Protran® Western-Blotting-Membrane, GE Healthcare Life science, Il, USA) and air-dried for 30 minutes at room temperature. Membrane was blocked in 5% (w/v) non-fat milk (AppliChem) in T-TBS for 1 hour, followed by incubation with an anti-MUC2 antibody (**Supplementary Table 6**) over night at 4°C. After two washes in T-TBS, membrane was incubated with Anti-rabbit IgG HRP (**Supplementary Table 6**) for 1 hour at room temperature and washed again. Signals were detected using SuperSignal™ West Atto Ultimate Sensitivity Chemiluminescent Substrate (ThermoScientific, #A38554) and visualized on the iBright™ CL1500 Imaging System (ThermoFisher). To determine equal transfer and loading, membranes were stripped and stained afterwards with Swift Membrane Stain™ (G-Biosciences, MO, USA, #786-677) to normalize the abundance of MUC2.

Histology and microscopy analyses

Immunohistochemical (IHC) staining in Formaldehyde (Th. Geyer BIOSOLUTE, Renningen, Germany) (FFPE)-fixed and paraffin-embedded murine colonic tissue biopsies was performed according to standard protocols. After deparaffinization, rehydration, endogenous peroxidase blockage, a blockage in 2% (w/v) BSA, and antigen retrieval, tissue slides were probed with specific primary antibodies or isotype control antibodies, followed by respective HRP-conjugated secondary antibodies or HRP-labelled polymers (listed in **Supplementary Table 6**). Tissue slides were incubated with DAB-substrate (Dako, Jena, Germany, #GV825) and counterstained with Haemalaune. Images were obtained and analysed on an Axio Scope.A1 microscope (Zeiss, Oberkochen, Germany) utilizing the ZEN imaging software (v2.3, Zeiss). If appropriate, stained areas were quantified using the colour deconvolution plugin for the software ImageJ software [69]. Crypt length was quantified using Zen imaging software (v2.3, Zeiss). Six complete colonic crypts sectioned longitudinally from base to apex were measured per mouse within one image, and the median value was calculated for analysis.

Lipidomic analysis of murine faecal samples

A Dionex Ultimate 3000 RS LC-system coupled to an Orbitrap mass spectrometer (QExactive, ThermoFisher Scientific, Bremen, Germany) equipped with a heated-electrospray ionization (HESI-II) probe was used. All solvents were of LC-MS grade quality and were purchased from Merck (Darmstadt, Germany). Collected faeces samples were homogenized in 150-500 µl water using a tissue homogenizer (Bullet Blender, Next Advance, NY, USA). After centrifugation (2000 *x* g/ 4°C/ 5 min), supernatants were diluted accordingly to reach a protein concentration between 0.5-1.2 mg/ml. Exact protein concentration was determined using a Bradford assay (Sigma-Aldrich, #B6916) according to the manufacturer's instruction. Lipid profiling was performed as described previously[70]. Briefly, lipids were extracted by adding 1 ml of methanol/methyl tertiary-butyl ether/chloroform (1.33:1:1, v/v), containing butylated hydroxytoluene (100 mg/l, Sigma-Aldrich, #B1378) and 2.5 ml/l of SPLASH internal standard mix (Avanti Polar Lipids, Alabaster, AL, USA, #330707), to 50 µl of tissue homogenate. After incubation and centrifugation, supernatants were dried under vacuum and resuspended in 50 µl of methanol/isopropyl alcohol (1:1, v/v) for LC-MS/MS analysis. Extracted lipids were separated on an Accucore C30 RP column (150 × 2.1 mm, 2.6 µm) using acetonitrile/water 6:4 v/v as eluent A and

isopropyl alcohol/acetonitrile (9:1, v/v) as eluent B; 10 mM ammonium acetate (Sigma-Aldrich, #A7330) and 0.1 % (v/v) formic acid (Biosolve, Dieuze, France, #069106) was added to both eluents. Ionization and data acquisition with data-dependent MS² scans (top 15) was performed as described previously [70,71]. Lipid species were identified based on an in-house database, according to exact mass, retention time, fragmentation ions, and isotopic pattern. The area under the peak was normalized to the internal standard and the protein concentration. Pooled samples at 5 concentrations were used as quality controls. In accordance with the 3R principle we analysed samples that were derived from a previously conducted experiments, therefore, stool samples from the 12-week mouse model were not available for analysis.

NMR metabolome analysis

Thawed aliquots of frozen serum samples were mixed 1:1 (v/v) with 75 mM sodium phosphate buffer (pH 7.4). 600 µL of the mixed samples were transferred into a 3 mm Nuclear Magnetic Resonance (NMR) tube. NMR analysis was conducted on a Bruker 600 MHz Avance III HD spectrometer with a TXI probe, using a Bruker SampleJetTM automatic sample changer with cooling set to 6°C. The experiments were performed following the Bruker *in vitro* Diagnostic Research (IVDr) protocol. To ensure quality control, the NMR spectrometer was calibrated daily using a strict standard operation procedure protocol based on the method described by Dona *et al.*[72]. For each sample, four different 1H NMR experiments were measured at 310 K. One-dimensional (1D) proton spectra were recorded using a standard Bruker pulse program (noesygppr1d) with pre-saturation water suppression during the 4-second recycle delay. Additionally, a 1D Carr-Purcell-Meiboom-Gill (CPMG) spin-echo experiment (pulseprogram: cpmgpr1d) was acquired to suppress proteins and other macromolecular signals. These spectra were obtained with 32 scans and 131,072 data points. Moreover, 2D J-resolved and diffusion-edited experiments were performed. From the acquired spectra, concentrations of 39 metabolites and 112 lipoproteins were automatically determined using B.I. Quant-PS 2.0.0 and the Bruker IVDr Lipoprotein Subclass Analysis B.I.-LISATM (Bruker BioSpin). Of note, results from this analysis were also used to determine TAG level in murine and human serum, as well as glucose concentrations in murine serum.

Enzyme-Linked Immunosorbent Assay (ELISA)

The serum C-peptide levels were measured using a C-peptide Enzyme Immunoassay Kit (RayBiotech, Norcross, USA), according to the manufacturer's instructions.

For determination of insulin concentrations in serum the Mouse Insulin ELISA Kit (Invitrogen, Waltham, USA, #EMINS) was used, following the instructions from the manufacturer. Only exception, the sample and standard volume was reduced to 30 µl per well.

The serum level of arachidonic acid was measured using an Arachidonic Acid Immunoassay Kit (Abcam, Cambridge, UK, # ab287798), according to the manufacturer's instructions.

To determine PGE_2 concentrations undiluted supernatants of organoids were applied to the Human Prostaglandin E2 ELISA Kit (Invitrogen, #KHL1701), according to the manufacturer's instructions.

For all ELISAs the absorbance was read, using a microplate reader (SpectraMax iD3, Molecular Devices, CA, USA).

D-Glucose assay

D-glucose levels were measured using the D-Glucose Assay Kit (Megazyme, #K-GLUC). D-Glucose levels were measured in supernatants from organoid culture diluted in ddH_2O. 5 µl of diluted sample, blank, and standards were added in duplicates into a 96-well plate. 150 µl GOPOD reagent was added to each well and the plate was incubated for 20 minutes at 45°C protected from light. Absorbance was read at 510 nm, using the SpectraMax iD3 (Molecular Devices).

Triglyceride assay

Glyceride levels in supernatants from organoid culture were measured using the Triglyceride Assay (Sigma Aldrich, #MAK266A). The assay was performed according to manufacturer's protocol, however using only half of the recommended volume and half area plates (Corning, #CLS3690). After 45-minute incubation samples were measured at 570 nm, using a microplate reader (SpectraMax iD3, Molecular Devices).

Triglyceride levels in plasma samples of the 12-week intervention animals were analysed by LC-MS, as published in a previous study [21].

Statistics

Statistical analysis and data visualization was performed using the GraphPad Prism version 10.2.1 (San Diego, California, US). No statistical method was used to predetermine sample sizes. Outliers were identified by Grubbs' test (significance level $\alpha = 0.05$). The F test was used to compare variances and D'Agostino-Pearson test was applied to test for normal distribution. Statistical differences between two groups were analysed by unpaired t-test or paired t-test (normally distributed data), unpaired t-test with Welch's correction (significantly different variances) or Mann-Whitney U-test (not-normally distributed data). Two-way analysis of variance (ANOVA) with Bonferroni's, Dunnett's, Šídák's, Tukey's, or Fisher's least significant difference (LSD) post hoc test was applied for datasets with two variables. Correlation analysis was performed by obtaining the Spearman's rank correlation coefficient. P-values were calculated, and null hypotheses were rejected when $p \leq 0.05$. Data are shown as median with range, as mean ± standard error of the mean (mean ± S.E.M.), or as mean ± standard deviation (mean ± S.D.).

References

1. Xi, Y. & Xu, P. Global colorectal cancer burden in 2020 and projections to 2040. *Transl. Oncol.* **14**, 101174 (2021).

2. Siegel, R. L. *et al.* Global patterns and trends in colorectal cancer incidence in young adults. *Gut* **68**, 2179–2185 (2019).

3. Arnold, M. *et al.* Global patterns and trends in colorectal cancer incidence and mortality. *Gut* **66**, 683–691 (2017).

4. Vuik, F. E. *et al.* Increasing incidence of colorectal cancer in young adults in Europe over the last 25 years. *Gut* **68**, 1820–1826 (2019).

5. Samuel, S. M., Varghese, E. & Büsselberg, D. Complexity of insulin resistance in early-onset colorectal cancer. *Cancer Cell* **43**, 797–802 (2025).

6. Liscovitch, M. & Cantley, L. C. Lipid second messengers. *Cell* **77**, 329–334 (1994).

7. DiNicolantonio, J. J. & O'Keefe, J. The Importance of Maintaining a Low Omega-6/Omega-3 Ratio for Reducing the Risk of Autoimmune Diseases, Asthma, and Allergies. *Mo. Med.* **118**, 453–459 (2021).

8. Simopoulos, A. P. The importance of the ratio of omega-6/omega-3 essential fatty acids. *Biomed. Pharmacother.* **56**, 365–379 (2002).

9. Ibarguren, M., López, D. J. & Escribá, P. V. The effect of natural and synthetic fatty acids on membrane structure, microdomain organization, cellular functions and human health. *Biochim. Biophys. Acta - Biomembr.* **1838**, 1518–1528 (2014).

10. Schwärzler, J. *et al.* PUFA-Induced Metabolic Enteritis as a Fuel for Crohn's Disease. *Gastroenterology* **162**, 1690–1704 (2022).

11. Aglago, E. K. *et al.* Consumption of Fish and Long-chain n-3 Polyunsaturated Fatty Acids Is Associated With Reduced Risk of Colorectal Cancer in a Large European Cohort. *Clin. Gastroenterol. Hepatol.* **18**, 654-666.e6 (2020).

12. Esser-von Bieren, J. Eicosanoids in tissue repair. *Immunol. Cell Biol.* **97**, 279–288 (2019).

13. Miyoshi, H. *et al.* Prostaglandin E2 promotes intestinal repair through an adaptive cellular response of the epithelium. *EMBO J.* **36**, 5–24 (2017).

14. Hiraide, T. *et al.* Accumulation of arachidonic acid-containing phosphatidylinositol at the outer edge of colorectal cancer. *Sci. Rep.* **6**, 1–11 (2016).

15. Gehart, H. & Clevers, H. Tales from the crypt: new insights into intestinal stem cells. *Nat. Rev. Gastroenterol. Hepatol.* **16**, 19–34 (2019).

16. Schell, J. C. *et al.* Control of intestinal stem cell function and proliferation by mitochondrial pyruvate metabolism. *Nat. Cell Biol.* **19**, 1027–1036 (2017).

17. Beerman, I., Seita, J., Inlay, M. A., Weissman, I. L. & Rossi, D. J. Quiescent hematopoietic stem cells accumulate DNA damage during aging that is repaired upon entry into cell cycle. *Cell Stem Cell* **15**, 37–50 (2014).

18. Li, W. *et al.* The nutritional environment determines which and how intestinal stem cells contribute to homeostasis and tumorigenesis. *Carcinogenesis* **40**, 937–946 (2019).

19. Augenlicht, L. H. Environmental Impact on Intestinal Stem Cell Functions in Mucosal Homeostasis and Tumorigenesis. *J. Cell. Biochem.* **118**, 943–952 (2017).

20. Wang, S., Lai, X., Deng, Y. & Song, Y. Correlation between mouse age and human age in anti-tumor research: Significance and method establishment. *Life Sci.* **242**, 117242 (2020).

21. Nickel, L. *et al.* The AT1 Receptor Blocker Telmisartan Reduces Intestinal Mucus Thickness in Obese Mice. *Front. Pharmacol.* **13**, 815353 (2022).

22. Kahn, A. R. S. & Ronald, C. Insulin signalling and the regulation of glucose and lipid

metabolism. *Nature* **414**, 799–806 (2001).

23. Hardie, D. G., Ross, F. A. & Hawley, S. A. AMPK: A nutrient and energy sensor that maintains energy homeostasis. *Nat. Rev. Mol. Cell Biol.* **13**, 251–262 (2012).

24. Shiwa, M. *et al.* Distinct Time Course of the Decrease in Hepatic AMP-Activated Protein Kinase and Akt Phosphorylation in Mice Fed a High Fat Diet. *PLoS One* **10**, e0135554 (2015).

25. Boden, G., Chen, X., Ruiz, J., White, J. V & Rossetti, L. Mechanisms of fatty acid-induced inhibition of glucose uptake . Mechanisms of Fatty Acid-induced Inhibition of Glucose Uptake. **93**, 2438–2446 (1994).

26. Dupaul-Chicoine, J. *et al.* Control of Intestinal Homeostasis, Colitis, and Colitis-Associated Colorectal Cancer by the Inflammatory Caspases. *Immunity* **32**, 367–378 (2010).

27. Sünderhauf, A. *et al.* GC1qR Cleavage by Caspase-1 Drives Aerobic Glycolysis in Tumor Cells. *Front. Oncol.* **10**, 575854 (2020).

28. Araki, K., Ogata, T., Kobayashi, M. & Yatani, R. A morphological study on the histogenesis of human colorectal hyperplastic polyps. *Gastroenterology* **109**, 1468–1474 (1995).

29. Wang, W. *et al.* Butyrate and propionate are microbial danger signals that activate the NLRP3 inflammasome in human macrophages upon TLR stimulation. *Cell Rep.* **43**, (2024).

30. Wen, H. *et al.* Fatty acid-induced NLRP3-ASC inflammasome activation interferes with insulin signaling. *Nat. Immunol.* **12**, 408–415 (2011).

31. Friedman, E. *et al.* Fecal Diglycerides as Selective Endogenous Mitogens for Premalignant and Malignant Human Colonic Epithelial Cells. *Cancer Res.* **49**, 544–548 (1989).

32. Mayr, L. *et al.* Dietary lipids fuel GPX4-restricted enteritis resembling Crohn's disease. *Nat. Commun.* **11**, (2020).

33. Xu, C. *et al.* FADS1-arachidonic acid axis enhances arachidonic acid metabolism by altering intestinal microecology in colorectal cancer. *Nat. Commun.* **14**, (2023).

34. Yates, C. M., Calder, P. C. & Ed Rainger, G. Pharmacology and therapeutics of omega-3 polyunsaturated fatty acids in chronic inflammatory disease. *Pharmacol. Ther.* **141**, 272–282 (2014).

35. Rae, S. A., Davidson, E. M. & Smith, M. J. H. Leukotriene B4, an Inflammatory Mediator in Gout. *Lancet* **320**, 1122–1124 (1982).

36. Villanueva, C. J. *et al.* Specific role for acyl CoA:diacylglycerol acyltransferase 1 (Dgat1) in hepatic steatosis due to exogenous fatty acids. *Hepatology* **50**, 434–442 (2009).

37. Lee, B., Fast, A. M., Zhu, J., Cheng, J.-X. & Buhman, K. K. Intestine-specific expression of acyl CoA:diacylglycerol acyltransferase 1 reverses resistance to diet-induced hepatic steatosis and obesity in Dgat1-/- mice. *J. Lipid Res.* **51**, 1770–1780 (2010).

38. Shin, M., Ware, T. B. & Hsu, K. L. DAGL-Beta Functions as a PUFA-Specific Triacylglycerol Lipase in Macrophages. *Cell Chem. Biol.* **27**, 314-321.e5 (2020).

39. Ding, L. *et al.* Peroxisomal β-oxidation acts as a sensor for intracellular fatty acids and regulates lipolysis. *Nat. Metab.* **3**, 1648–1661 (2021).

40. Barker, N., Van Oudenaarden, A. & Clevers, H. Identifying the stem cell of the intestinal crypt: Strategies and pitfalls. *Cell Stem Cell* **11**, 452–460 (2012).

41. CZI Single-Cell Biology. No Title. *CELLxGENE: a performant, scalable exploration platform for high dimensional sparse matrices* bioRxiv 2021.04.05 doi:https://doi.org/10.1101/2021.04.05.438318.

42. Roig, A. I. *et al.* Immortalized Epithelial Cells Derived From Human Colon Biopsies Express Stem Cell Markers and Differentiate In Vitro. *Gastroenterology* **138**, 1012-1021.e5 (2010).

43. Fordham, R. P. *et al.* Transplantation of expanded fetal intestinal progenitors contributes to colon regeneration after injury. *Cell Stem Cell* **13**, 734–744 (2013).

44. Mustata, R. C. *et al.* Identification of Lgr5-independent spheroid-generating progenitors of the mouse fetal intestinal epithelium. *Cell Rep.* **5**, 421–432 (2013).

45. Wang, Q. *et al.* Arachidonic Acid Promotes Intestinal Regeneration by Activating WNT Signaling. *Stem cell reports* **15**, 374–388 (2020).

46. Nakanishi, M. & Rosenberg, D. W. Multifaceted roles of PGE2 in inflammation and cancer. *Semin. Immunopathol.* **35**, 123–137 (2013).

47. Park, J. Y., Pillinger, M. H. & Abramson, S. B. Prostaglandin E2 synthesis and secretion: the role of PGE2 synthases. *Clin. Immunol.* **119**, 229–240 (2006).

48. Sachdev, V. *et al.* Novel role of a triglyceride-synthesizing enzyme: DGAT1 at the crossroad between triglyceride and cholesterol metabolism. *Biochim. Biophys. Acta* **1861**, 1132–1141 (2016).

49. Lombardo, Y. B. *et al.* Long-term administration of a sucrose-rich diet to normal rats: relationship between metabolic and hormonal profiles and morphological changes in the endocrine pancreas. *Metabolism.* **45**, 1527–1532 (1996).

50. Coelho, M. S. *et al.* High sucrose intake in rats is associated with increased ACE2 and angiotensin-(1-7) levels in the adipose tissue. *Regul. Pept.* **162**, 61–67 (2010).

51. Li, C. *et al.* Glycolytic Regulation of Intestinal Stem Cell Self-Renewal and Differentiation. *Cell. Mol. Gastroenterol. Hepatol.* **15**, 931–947 (2023).

52. He, X., Semenov, M., Tamai, K. & Zeng, X. LDL receptor-related proteins 5 and 6 in Wnt/β-catenin signaling:Arrows point the way. *Development* **131**, 1663–1677 (2004).

53. Desbois-Mouthon, C. *et al.* Insulin and IGF-1 stimulate the beta-catenin pathway through two signalling cascades involving GSK-3beta inhibition and Ras activation. *Oncogene* **20**, 252–259 (2001).

54. Sasaki, N. *et al.* Reg4+ deep crypt secretory cells function as epithelial niche for Lgr5+ stem cells in colon. *Proc. Natl. Acad. Sci. U. S. A.* **113**, E5399-407 (2016).

55. Burclaff, J. *et al.* A Proximal-to-Distal Survey of Healthy Adult Human Small Intestine and Colon Epithelium by Single-Cell Transcriptomics. *Cmgh* **13**, 1554–1589 (2022).

56. Tümpel, S. & Rudolph, K. L. Quiescence: Good and Bad of Stem Cell Aging. *Trends Cell Biol.* **29**, 672–685 (2019).

57. Andersen, C. J., Murphy, K. E. & Fernandez, M. L. Impact of Obesity and Metabolic Syndrome on Immunity. *Adv. Nutr.* **7**, 66–75 (2016).

58. Harlid, S., Myte, R. & Van Guelpen, B. The Metabolic Syndrome, Inflammation, and Colorectal Cancer Risk: An Evaluation of Large Panels of Plasma Protein Markers Using Repeated, Prediagnostic Samples. *Mediators Inflamm.* **2017**, (2017).

59. Cox, A. J., West, N. P. & Cripps, A. W. Obesity, inflammation, and the gut microbiota. *lancet. Diabetes Endocrinol.* **3**, 207–215 (2015).

60. Esposito, K., Chiodini, P., Colao, A., Lenzi, A. & Giugliano, D. Metabolic syndrome and risk of cancer: a systematic review and meta-analysis. *Diabetes Care* **35**, 2402–2411 (2012).

61. Petersen, M. C. & Shulman, G. I. Mechanisms of Insulin Action and Insulin Resistance. *Physiol. Rev.* **98**, 2133–2223 (2018).

62. Ostermann, A. L. *et al.* Intestinal insulin/IGF1 signalling through FoxO1 regulates epithelial integrity and susceptibility to colon cancer. *Nat. Metab.* **1**, 371–389 (2019).

63. Ito, K. & Suda, T. Metabolic requirements for the maintenance of self-renewing stem cells. *Nat. Rev. Mol. Cell Biol.* **15**, 243–256 (2014).

64. Andres, S. F. *et al.* Deletion of intestinal epithelial insulin receptor attenuates high-fat diet-induced elevations in cholesterol and stem, enteroendocrine, and Paneth cell mRNAs. *Am. J. Physiol. Gastrointest. Liver Physiol.* **308**, G100-11 (2015).

65. Mills, J. C. & Sansom, O. J. Reserve stem cells: Differentiated cells reprogram to fuel repair, metaplasia, and neoplasia in the adult gastrointestinal tract. *Sci. Signal.* **8**, re8 (2015).

66. Tallima, H. & El Ridi, R. Arachidonic acid: Physiological roles and potential health benefits - A review. *J. Adv. Res.* **11**, 33–41 (2018).

67. Hyde, C. A. C. & Missailidis, S. Inhibition of arachidonic acid metabolism and its implication on cell proliferation and tumour-angiogenesis. *Int. Immunopharmacol.* **9**, 701–715 (2009).

68. Peregrina, K. *et al.* Vitamin D is a determinant of mouse intestinal Lgr5 stem cell functions. *Carcinogenesis* **36**, 25–31 (2015).

69. Ruifrok, A. C. & Johnston, D. A. Quantification of histochemical staining by color deconvolution. *Anal. Quant. Cytol. Histol.* **23**, 291–299 (2001).

70. Aherrahrou, R. *et al.* CYP17A1 deficient XY mice display susceptibility to atherosclerosis, altered lipidomic profile and atypical sex development. *Sci. Rep.* **10**, 1–11 (2020).

71. Karsai, G. *et al.* DEGS1-associated aberrant sphingolipid metabolism impairs nervous system function in humans. *J. Clin. Invest.* **129**, 1229–1239 (2019).

72. Dona, A. C. *et al.* Precision high-throughput proton NMR spectroscopy of human urine, serum, and plasma for large-scale metabolic phenotyping. *Anal. Chem.* **86**, 9887–9894 (2014).

Acknowledgements

The authors thank all the participating patients for contributing to this study, Dr. Julica Inderhees and Prof. Olaf Jöhren for providing the LC/MS based lipidomic platform, and Prof. Dr. Ulrich Günther for providing the NMR metabolomics platform. Furthermore, we would like to thank Dr. Damian Graczyk and Prof. Dr. Jerry W. Shay for sharing the HCEC-1CT.

Author contributions

SDe designed the concept of the study and supervised it. MR, SDe, SDi, LN, WR, LJ, DC and JUM designed, supervised, and performed the animal experiments and provided the murine colon and serum samples. TG collected serum samples of patients with CRC and SDe, ST and LC collected and provided human biopsies for organoid generation and serum of patients without CRC. LC, SDe, MH, HS, RW, FS, DM, SM, IR, HW and NB performed the experiments and acquired the data. LA, CG, AR, DV and CS provided expertise in the field and offered critical feedback on the discussion of the study results. LC and SDe analysed and interpreted the data and drafted the article. All authors read and approved the final manuscript.

Competing interests

The authors declare no conflicts of interest.

Figure 1

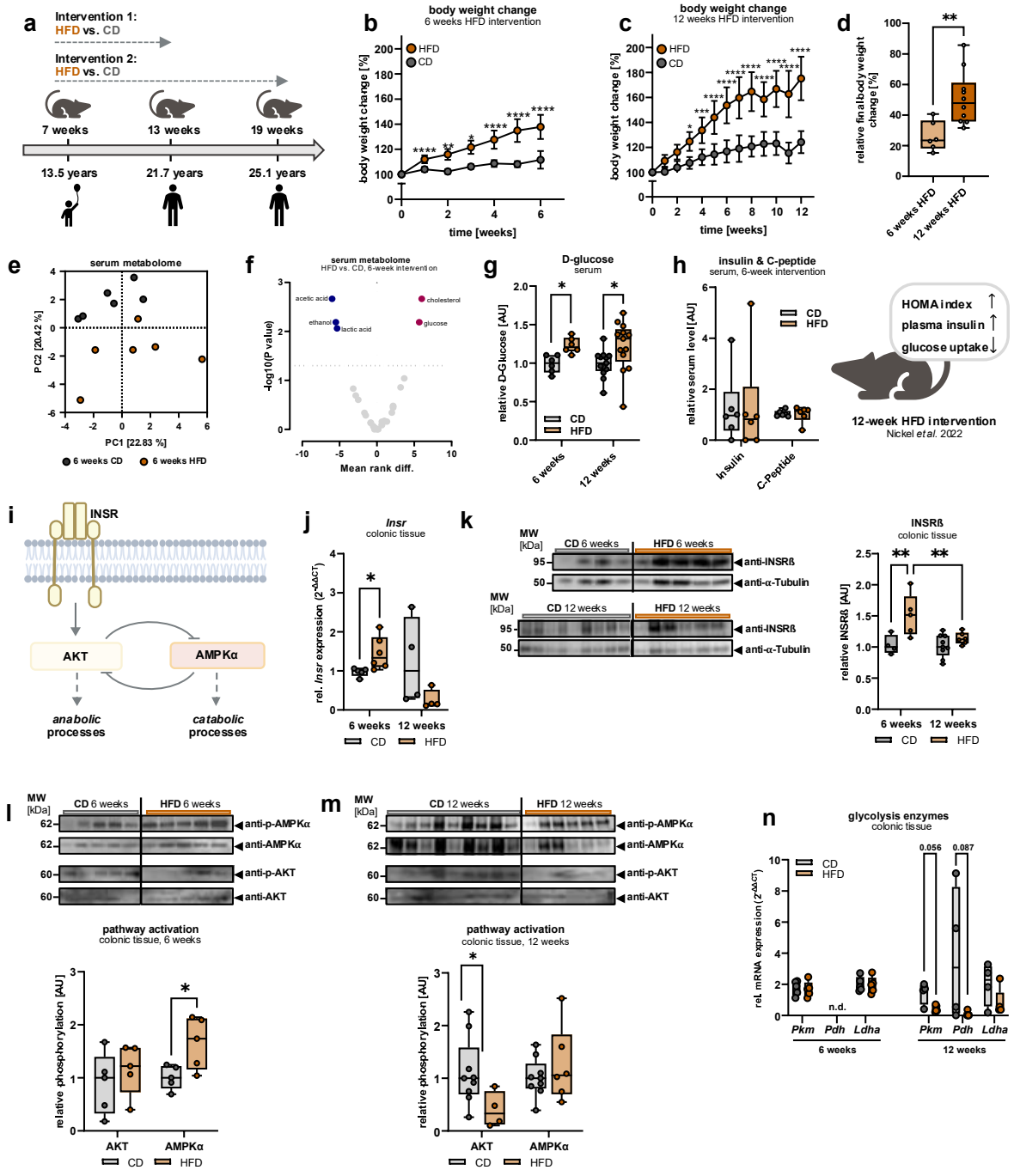


Fig. 1 | Insulin resistance is associated with the onset of colonic EC insulin resistance in mice. **(a)** Schematic overview of two independent HFD-mouse models (6 weeks n=6 per group; 12 weeks n=13 per group) with equivalent human age calculation based on Wang *et al.*[20]. **(b)+(c)** Time-dependent change of body weight [%] of mice fed for 6 weeks (n=6 per group) or 12 weeks (n=13 per group). **(d)** Comparison of final body weight increase [%] under HDF-feeding relative to CD between mice on HFD for 6 weeks (n=6) or 12 weeks (n=10). **(e)** Principal component analysis (PCA) of metabolites measured in serum samples of HFD-fed (brown, n=6) and CD-fed (grey, n=6) mice after 6 weeks intervention, using 1H nuclear magnetic resonance (NMR) spectroscopy *in-vitro* Diagnostic Research (IVDr) metabolomics. **(f)** Volcano plot of differentially abundant metabolites in serum (n=6 per group) of mice after 6 weeks (red: significantly increased, blue: significantly decreased) identified by NMR IVDr metabolomics, displaying unadjusted *P*-values. **(g)** Relative D-glucose concentration in serum of mice after 6 weeks (n=6 per group) and 12 weeks (n=13 per group). **(h) Left:** Relative insulin and C-peptide

concentration in serum of mice after 6 weeks intervention (HFD n=6, CD n=6). **Right:** schematic summary of insulin status in mice after 12 weeks[21]. **(i)** Scheme depicting the main insulin receptor downstream signalling pathway. **(j)** Relative expression of *Insr* in murine colonic tissue of HFD-fed mice compared to CD-fed littermates (6 weeks: HFD n=6, CD n=5; 12 weeks: HFD n=4, CD n=4), displaying adjusted *P*-values. **(k) Left:** INSRβ detection in murine colonic tissue after 6 weeks (HFD n=5, CD n=4) and after 12 weeks (HFD n=6, CD n=9) via Western blotting. **Right**: INSRβ quantification in colonic tissue of mice after 6- or 12-week HFD-feeding (6 weeks n=5; 12 weeks n=6) relative to CD-fed controls (6 weeks n=4; 12 weeks n=9) *via* Western blotting. **(l) Top:** Phosphorylation status of AKT, p44/42 (MAPK), and AMPKα in murine colonic tissue after 6 weeks (n=5 per group) *via* Western blot analysis. **Bottom:** Relative quantification of phosphorylation status (of AKT, and AMPKα in murine colonic tissue after 6 weeks (n=5 per group). **(m) Top:** Western blot analysis of phosphorylation status of AKT, and AMPKα in 12-week dietary intervention (HFD n=6, CD n=9). **Bottom:** Quantification of relative phosphorylation status after 12-week dietary intervention (HFD n=4-6, CD n=9). **(n)** Relative expression of glycolytic enzymes in murine colonic tissue after 6-week (HFD n=5-6; CD n=5) and 12-week (HFD n=5, CD n=4) intervention measured by RT-qPCR, displaying unadjusted *P*-values. **(b)-(c)** Two-way ANOVA with Šidák multiple comparisons test or **(g)-(h)**, **(k)-(n)** Fisher's least significant difference (LSD) test; **(d)**, **(f)**, **(j)** (Multiple) Mann-Whitney *U* test. **(b)-(c)** Data shown as mean ±S.D. and **(d)**, **(g)-(h)**, **(j)-(n)** box plots depicting the median and IQR with whiskers indicating the range with relative values determined by normalization to the median of the respective control group (set to 1). **P*≤0.05, ***P*≤0.01, ****P*≤0.001, *****P*≤0.0001. CD, control diet; Insr, insulin receptor; HFD, high-fat diet; IQR, interquartile range; Ldha, lactate dehydrogenase A; Pdh, pyruvate dehydrogenase; Pkm, pyruvate kinase isozyme M; S.D., standard deviation.

Figure 2

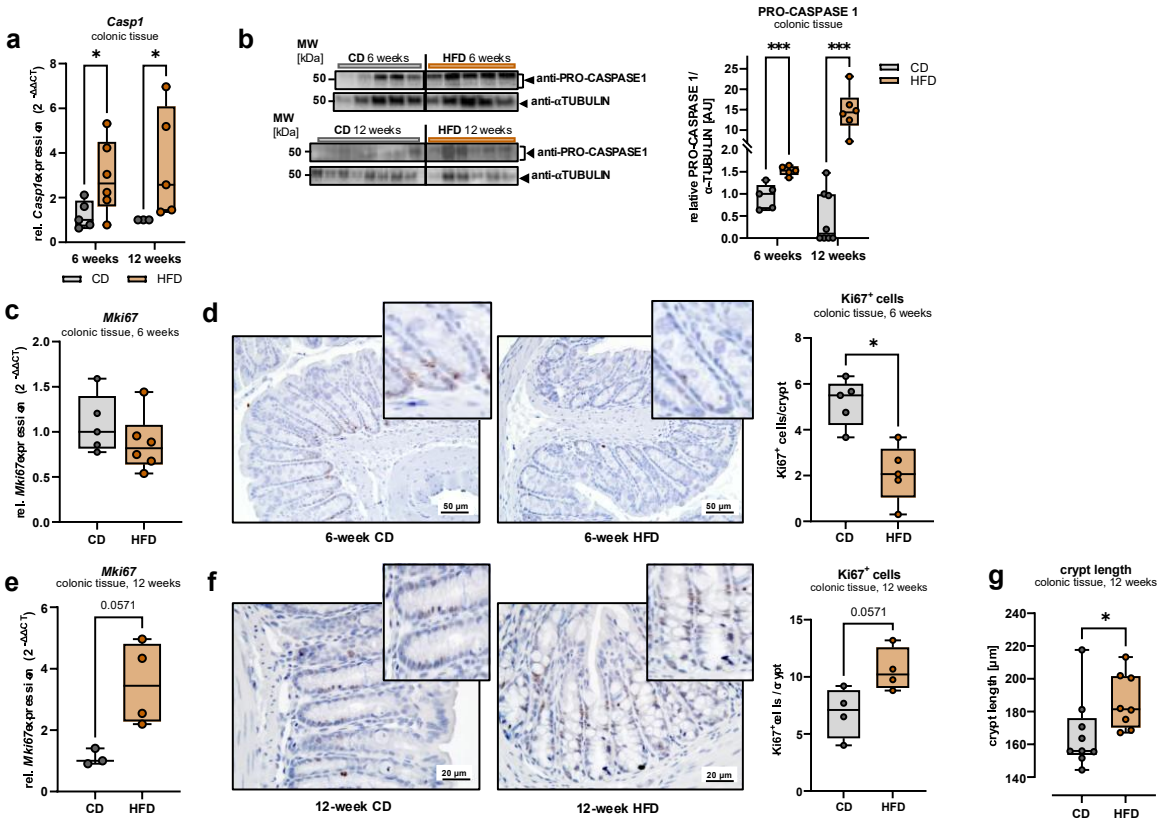


Fig. 2 | Colonic epithelial insulin resistance in young adult mice is associated with inflammation and hyperproliferation. (a) Relative expression of caspase-1 mRNA (*Casp1)* in murine colonic tissue after 6-week (HFD n=6, CD n=5) and 12-week (HFD n=5, CD n=3) intervention measured by RT-qPCR. **(b) Left:** Detection of colonic CASP1 level in mice after 6-week (HFD n=5, CD n=5) and 12-week (HFD n=6, CD n=8) dietary intervention using Western blotting. **Right:** Quantification of colonic CASP1 in HFD-fed mice (6-week n=5; 12-week n=6) and CD-fed mice (6-week n=5, 12-week n=8). **(c)** Relative expression of *Mki67* in murine colonic tissue after 6 weeks of dietary intervention (HFD n=6, CD n=5) measured by RT-qPCR. **(d) Left:** Representative images of IHC staining of murine colonic Ki67 after 6-week dietary intervention. **Right:** Total epithelial Ki67-staining in the colonic tissue of mice after 6-week dietary intervention quantified and normalized to crypt count (HFD n=5, CD n=5). **(e)** Relative expression of *Mki67* in murine colonic tissue after 12-week dietary intervention (HFD n=4, CD n=3) measured by RT-qPCR. **(f) Left:** Representative images of IHC staining of colonic Ki67 after 12 weeks dietary intervention. **Right**: Total epithelial Ki67 staining in colonic tissue quantified and normalized to crypt count (HFD n=4, CD n=4). **(g)** Colonic crypt length in mice measured from H&E-stained sections. **(a)-(b)** Two-way ANOVA with Šídák's multiple comparisons test; **(c)-(g)** Mann-Whitney *U* test. Box plots depict the median and IQR with whiskers indicating the range. All relative values were determined by normalization to the median of the respective control group (set to 1). **P*≤0.05, ****P*≤0.001. IQR, interquartile range.

Figure 3

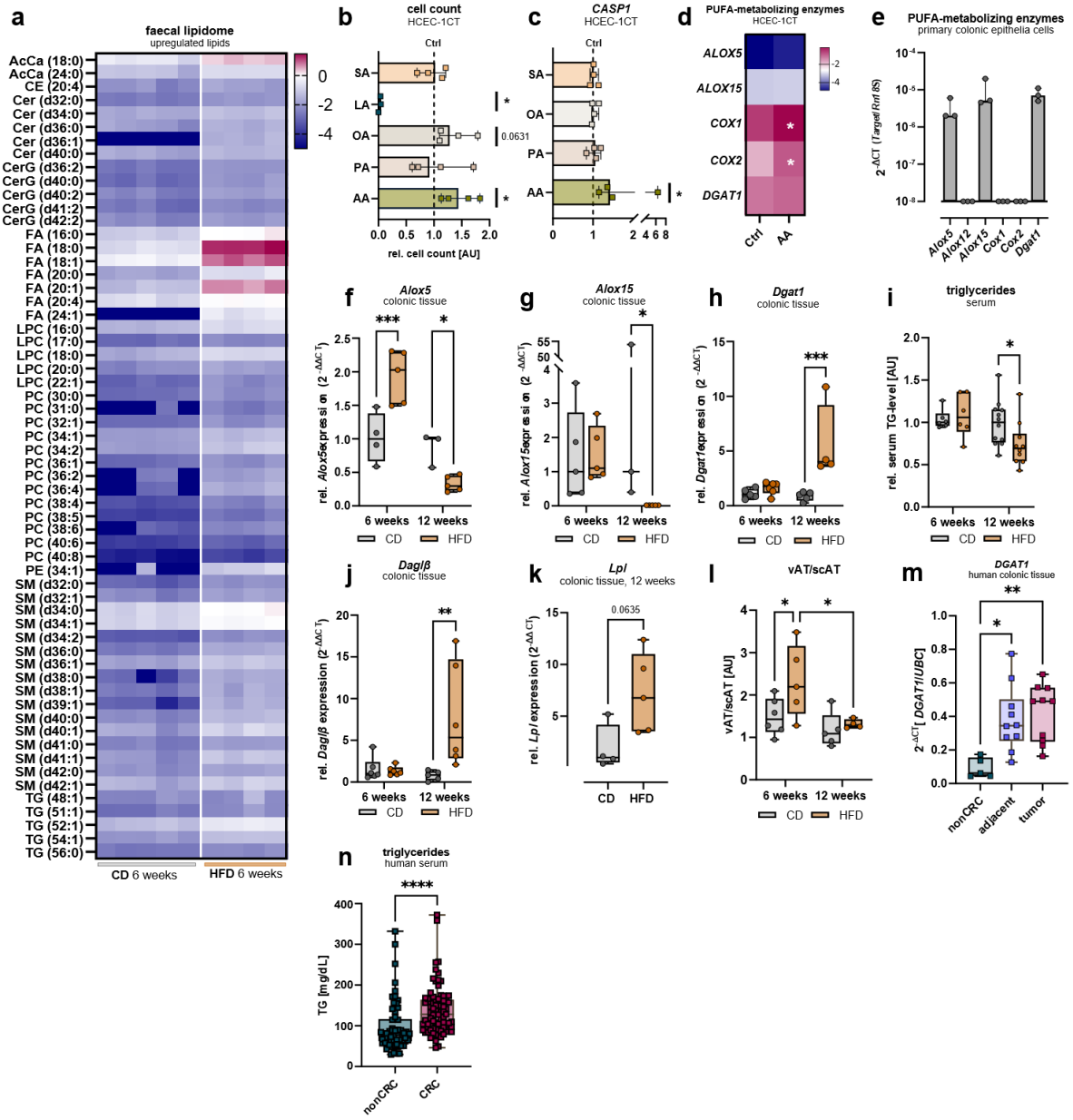


Fig. 3 | Insulin-resistant colonic epithelium redirects ω6-PUFA metabolism toward *Dgat1*- and *Daglβ*-dependent triglyceride turnover. (a) Significantly upregulated lipids in faecal samples of mice after 6-week HFD (n=4) in comparison to CD (n=5). **(b)** Relative cell count of the human non-cancerous cell line HCEC-1CT stimulated with 10 μM SA, OA, PA, AA (each group n=4) or LA (n=3), and compared to the respective control conditions set to 1 (Ctrl; ≤0.1% (v/v) EtOH, H_2O, or DMSO; n=4 each). **(c)** Relative *CASP1* expression of FA-treated HCEC-1CT (n=4 each group) in comparison to the respective control treatment (Ctrl; each group n=4). **(d)** Expression of PUFA-metabolizing enzymes in Ctrl-treated (n=5) and AA-treated (n=5) HCEC-1CT quantified using RT-qPCR and depicted as log-transformed $2^{-\Delta CT}$. **(e)** PUFA-metabolizing enzyme expression in primary colonic epithelial cells (pCECs) from mice (n=3). Relative colonic expression of **(f)** *Alox5* (6 weeks: HFD n=5, CD n=4; 12 weeks: HFD n=5, CD n=3), **(g)** *Alox15* (6 weeks: HFD n=5, CD n=5; 12 weeks: HFD n=5, CD n=3), and **(h)** *Dgat1* (6 weeks: HFD n=6, CD n=5; 12 weeks: HFD n=4, CD n=5) in mice after 6- and 12-week HFD intervention. **(i)** Relative serum triglyceride concentration in murine serum after 6-week (HFD n=6; CD n=6) and 12-week (HFD n=10; CD n=12) intervention. **(j)** Relative colonic expression of *Daglβ* after 6-week (HFD n=6, CD n=6) or 12-week (HFD n=6, CD n=5) intervention period. **(k)** Relative *Lpl* expression after 12-week intervention (HFD n=5, CD n=4). **(l)** Visceral fat (vAT) to subcutaneous fat (scAT) ratio after 6-

week (HFD n=5, CD n=6) and 12-week (HFD n=4, CD n=5) nutritional intervention. **(m)** Expression pattern of *DGAT1* in age-matched human colonic biopsies from hospitalized normal patients (nonCRC, n=5) and non-cancerous tissue adjacent to tumour side (adjacent, n=10) and paired tumour tissue (tumour, n=10) from Origene. **(n)** Quantification of triglyceride level in human serum of patients with CRC (CRC, n=79) compared to nonCRC (n=61), determined using NMR *IVDr* metabolomics. **(a)-(c)**, **(f)-(j)**, **(l)** Two-way ANOVA with Fisher's least significant difference (LSD) test. **(m)** Kruskal-Wallis test with Dunn's multiple comparisons test. **(d)**, **(k)**, **(n)** (Multiple) Mann-Whitney *U* test. Heatmap values in **(a)** shown as log-transformed individual data point [AU] and **(d)** values shown as median. **(b)**, **(c)**, **(e)** Bar graphs shown as median with error bars indicating the range. **(f)-(n)** Box plots depict the median and IQR with whiskers indicating the range. **(b)-(c)** Relative values were calculated by normalizing to the paired control condition (set to 1). **(f)-(k)** Relative values were determined by normalization to the median of the respective control group (set to 1). **P*≤0.05, ***P*≤0.01, ****P*≤0.001, *****P*≤0.0001. AA, arachidonic acid; CD, control diet; Ctrl, control; CRC, colorectal cancer; FA, fatty acid; HFD, high-fat diet; IQR, interquartile range; LA, linoleic acid; OA, oleic acid; PA, palmitic acids; SA, stearic acid.

Figure 4

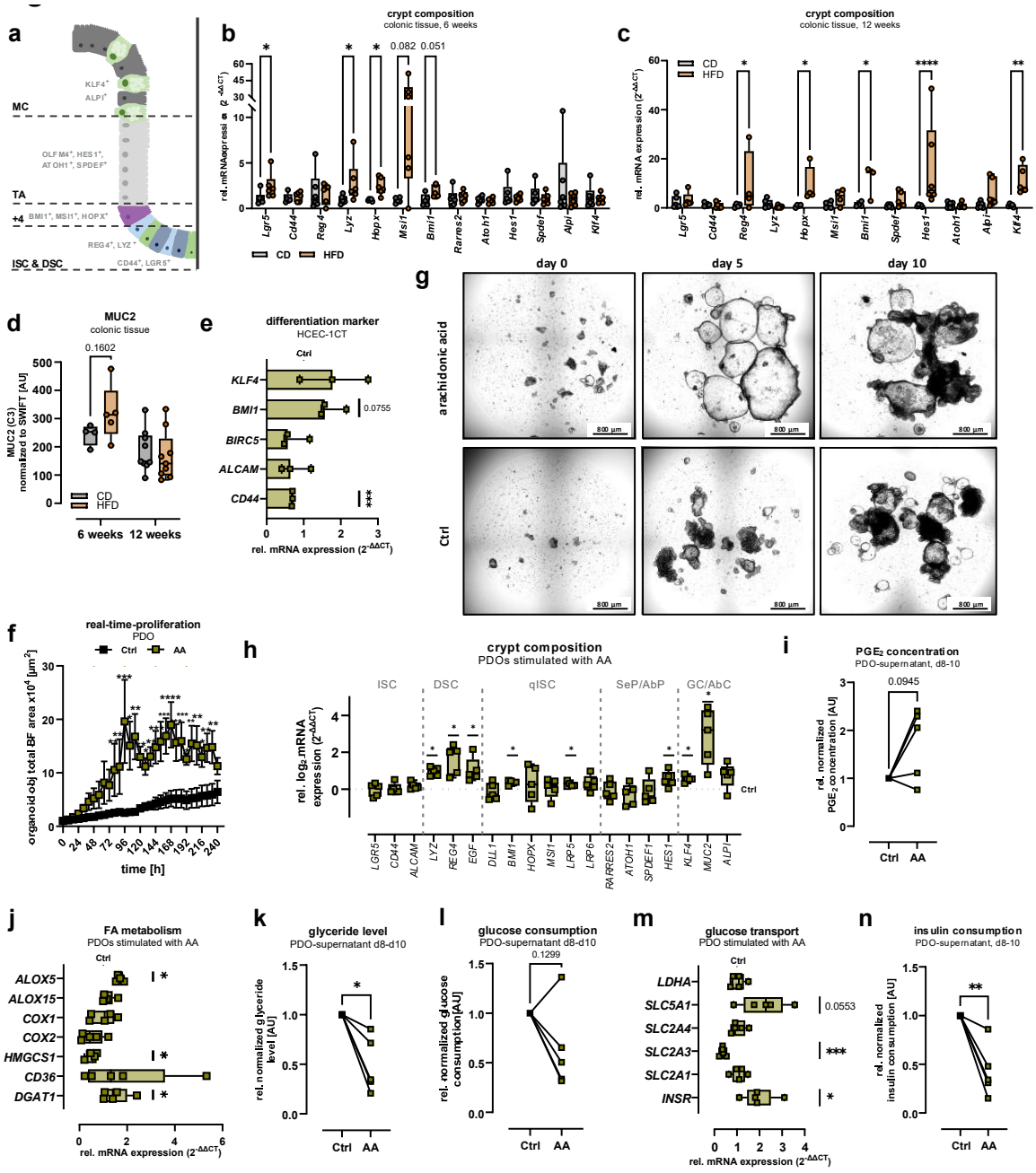


Fig. 4 | ω6-PUFA overload limits glucose uptake and LGR5⁺ ISC proliferation while expanding qISCs. (a) Illustration of the colonic crypt composition. **(b)** Relative expression of colonic crypt markers in colonic tissue of mice after 6-week HFD (n=5-6) compared to CD (n=5-6). **(c)** Expressional comparison of colonic crypt markers in colonic tissue of mice between HFD (n=3-6) and CD (n=5-6) after 12-week dietary intervention. **(d)** Normalized quantification of MUC2 in colonic tissue of HFD and CD mice after 6 weeks (HFD n=5, CD n=4) and 12 weeks (each group n=9). **(e)** Transcriptional differentiation profile of AA-stimulated HCEC-1CT cells (n=3) relative to DMSO-treated controls (Ctrl, n=3). **(f)** Paired real-time proliferation of human colonic organoids from healthy (nonCRC) patients treated with AA (n=5) or Ctrl (n=5), depicting Brightfield Area x 10^4 [µm²] captured every eight hours, normalized to day 0 with medium exchange indicated by dotted vertical lines. **(g)** Representative brightfield microscopy images of human colonic organoids at initiation (day 0), on day 5, and on day 10 of AA stimulation or Ctrl (4x magnification). **(h)** Log_2-transformed relative expression of AA-treated healthy human colonic organoids (n=5) compared to paired DMSO-treated controls (Ctrl, n=5). **(i)** Relative normalized prostaglandin E2 (PGE2) concentration quantified in the supernatant of day 8 to

day 10 (d8-10) from AA-treated (n=5) and compared to paired DMSO-treated (Ctrl, n=5) organoids. **(j)** Expression of different enzymes of the FA-metabolism quantified in AA-treated human colonic organoids from nonCRC patients (n=5) relative to paired DMSO-treated controls (Ctrl, n=5) using RT-qPCR. **(k)** Relative normalized glyceride levels and **(l)** relative normalized D-glucose consumption were quantified in the supernatant of d8-10 from AA-treated human colonic organoids from nonCRC patients (n=5) and compared to paired DMSO-treated organoids (Ctrl, n=5). **(m)** RT-qPCR analysis of enzymes important for glycolytic activity in AA-treated human colonic organoids (n=5) relative to paired DMSO-treated controls (Ctrl, n=5). **(n)** Relative normalized insulin consumption quantified in the supernatant of d8-10 from AA-treated human healthy colonic organoids (n=5) and compared to paired DMSO-treated organoids (Ctrl, n=5). **(b)**, **(e)**, **(h)**, **(j)** Multiple Mann-Whitney *U* test with unadjusted *P*-values. **(c)**, **(d)**, **(f)**, **(m),** Two-way ANOVA with Fisher's least significant difference (LSD) test. **(i)**, **(k)-(l)**, **(n)** Paired student's t-test. **(b)-(d)**, **(h)**, **(j)**, **(m)** Box plots depict the median and IQR with whiskers indicating the range, **(e)** data shown as median ± range and **(f)** as mean ± S.E.M.. **(b)-(d)** Relative values were determined by normalization to the median of the respective control group (set to 1); **(e)**, **(h)-(n)** relative values were calculated by normalizing to the paired control condition (set to 1). **P*≤0.05, ***P*≤.01, ****P*≤0.001, *****P*≤0.0001. AbC, absorptive enterocyte; AbP, absorptive progenitor; Ctrl, control; DSC, deep secretory cell; FA, fatty acid; GC, goblet cell; PDO, patient-derived organoid; ISC, intestinal stem cell; IQR, interquartile range; qISC, quiescent stem cell; S.E.M, standard error of the mean; SeP, secretory progenitor.

Figure 5

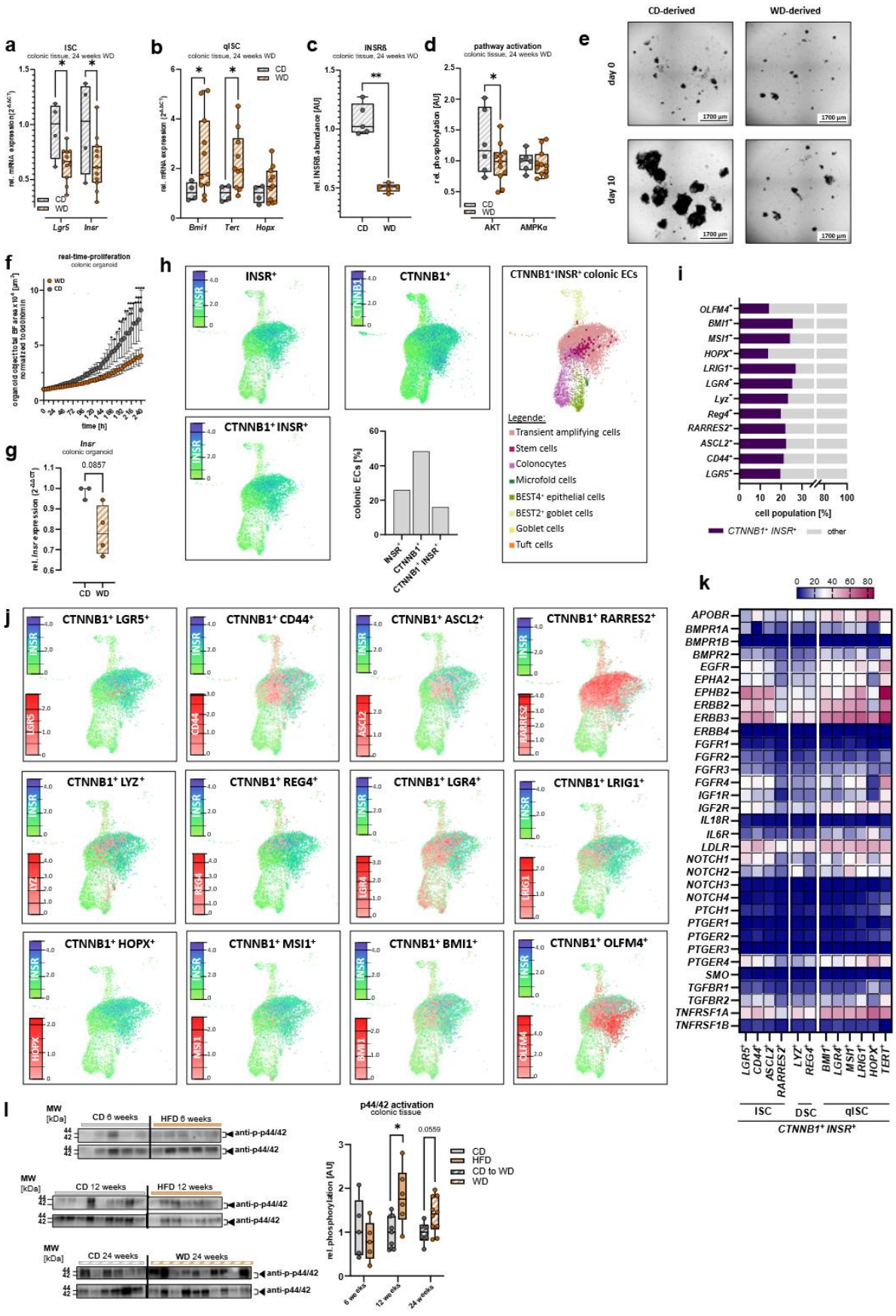


Fig. 5 | LGR5⁺ ISCs require INSR signalling for proliferation, whereas qISCs depend on growth factor and lipid pathways. (a) Expression of *Lgr5*, *Insr* and **(b)** *Bmi1*, *Tert*, and *Hopx* quantified in

colonic tissue from WD-fed (n=10-11) relative to CD-fed (n=4) mice using RT-qPCR. **(c)** INSRβ quantification in colonic tissue of WD-mice (n=5) relative to CD-fed controls (n=5) *via* Western blotting. **(d)** Relative phosphorylation status of AKT, and AMPKα in murine colonic tissue (WD n=11, CD n=6) determined by Western blot analysis. **(e)** Representative brightfield microscopy images of murine colonic organoids derived from WD- and CD-fed mice at day 0 and day 10 of basal cultivation (4x magnification). **(f)** Real-time proliferation of WD- (n=4) and CD-derived (n=3) organoids, depicting Brightfield Area x 10^4 [µm²] captured every 6 hours and normalized to day 0. **(g)** Relative expression of *Insr* in murine WD-derived colonic organoids (n=4) and CD-derived murine colonic organoids (n=3). **(h)** *INSR* and *CTNNB1* expression profile in colonic single-cell transcriptomics data of colonic tissue from healthy human adults[41]. **(i)** Proportion [%] of *CTNNB1*$^+$*INSR*$^+$ cells across lower crypt , based on single-cell transcriptomics data of colonic tissue from healthy human adults[41]. **(j)** Panels illustrate cells (red scale) expressing ISC-, qISC-, and DSC-specific markers co-expressed within *CTNNB1*$^+$ and *INSR*$^+$ (expression of INSR in green-blue scale), derived from single-cell transcriptomics profiles of healthy human adult colon[41]. **(k)** Heatmap of single-cell transcriptomics data from healthy human colon showing *CTNNB1*$^+$*INSR*$^+$ cells expressing ISC-, qISC, DSC-specific markers, and co-expressing a characteristic growth factor receptor signature. **(l) Left:** Western blot analysis of (phosphorylated) p44/42 (MAPK) after 6 weeks (HFD n=5, CD n=5), 12 weeks (HFD n=9, CD n=9) and after 24 weeks (CD n=6, WD n=10) of dietary intervention. **Right:** Relative phosphorylation status of MAPK downstream effector p44/42 (6 weeks: HFD n=5, CD n=5; 12 weeks: HFD n=6, CD n=9; 24 weeks: WD n=10, CD n=6). **(a)**,**(b)**,**(d)**,**(f)** Two-way ANOVA with Fisher's least significant difference (LSD) test. **(c)**, **(g)**, **(l)** (Multiple) Mann-Whitney *U* test with unadjusted *P*-values. **(a)-(d)**,**(g)**,**(l)** Box plots depict the median and IQR with whiskers indicating the range. **(f)** Data shown as mean ± S.E.M., and **(h)**,**(i)**,**(k)** as parts of a whole [%]. Relative values were determined by normalization to the median of the respective control group (set to 1). *P≤0.05, **P≤0.01, ***P≤0.001, ****P≤0.0001. Single-cell transcriptomics data of colonic healthy human adults publicly available in the Human Gut Cell Atlas[41]. IQR, interquartile range; S.E.M., standard error of the mean; WD, western-style diet.

Figure 6

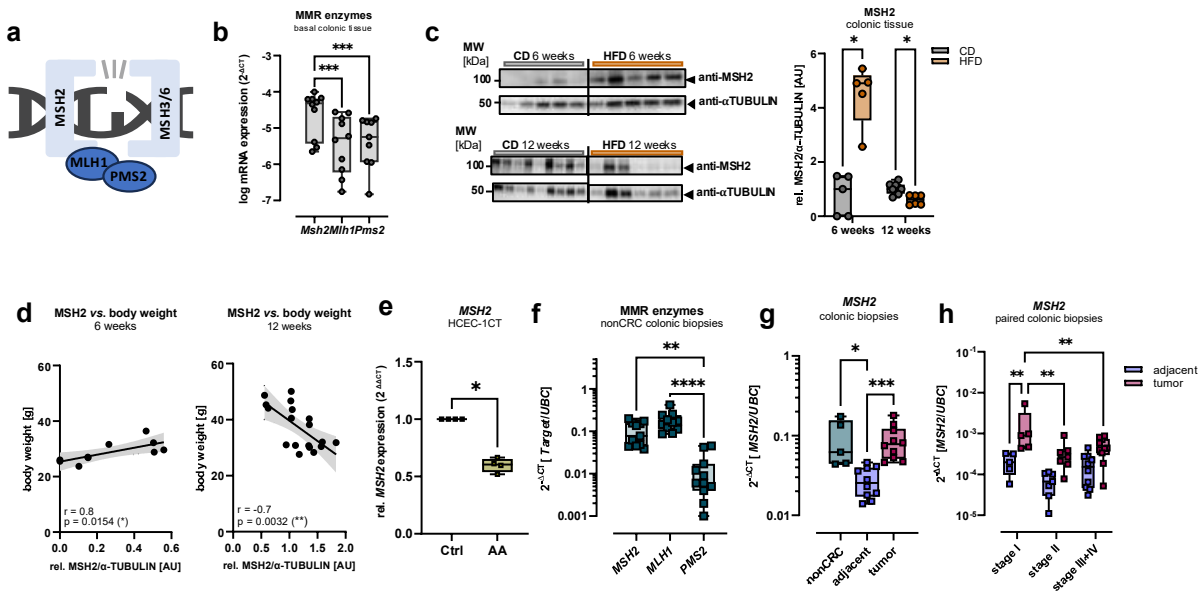


Fig. 6 | Colonic expansion of inherently DNA mismatch-prone qISC is linked to downregulation of MSH2. (a) Illustration of DNA mismatch repair (MMR) complex. **(b)** Log-transformed $2^{-\Delta CT}$ values of MMR complex components in basal murine colonic tissue (n=10). **(c) Left:** Western blot analysis using an anti-MSH2 antibody on colonic tissue from HFD- and CD-fed mice after 6 weeks (n=5 per group) and 12 weeks (HFD n=6, CD n=9), with α-Tubulin serving as loading control. **Right**: Quantification of MSH2 abundance in murine colonic tissue of HFD-fed mice relative to CD-fed littermates (6 weeks: n=5 per group; 12 weeks: HFD n=6, CD n=9). **(d)** Correlation of MSH2 level in murine colonic tissue with final body weight after 6 weeks (left; n=8) and after 12 weeks (right; n=18). **(e)** Expression of *MSH2* in human non-cancerous HCEC-1CT cells treated with 10µM AA (n=4) relative to DMSO-treated cells (n=4). **(f)** Basal expression of MMR complex enzymes in human colonic biopsies of hospitalized normal patients (nonCRC; n=11). **(g)** Basal expression of *MSH2* in age-matched human colonic biopsies from hospitalized normal tissue (nonCRC n=5), as well as paired non-cancerous tissue adjacent to tumour side (adjacent, n=10) and tumour tissue (tumour, n=10) from OriGene. **(h)** MSH2 expression in human colonic tumour (n=5) and paired adjacent (n=5) tissues (OriGene, #HCRT10303), stratified by UICC stage I (n=5 per group), II (n=7per group), and III+IV (n=10 per group). **(b)** Two-way ANOVA with Dunnett's test or **(c)**, **(h)** with Fisher's least significant difference (LSD) test. **(d)** Spearman correlation and linear regression with 95% confidence interval (dashed lines). **(e)** Mann-Whitney *U* test. **(f)-(g)** Kruskal-Wallis test with Dunn's multiple comparisons test. **(b)-(c)**, **(e)-(h)** Box plots depict the median and IQR with whiskers indicating the range. **(f)-(g)** Data shown on logarithmic y-axis. **(b)-(c)** Relative values were determined by normalization to the median of the respective CD control group (set to 1), **(e)** relative values were calculated by normalizing to the paired control condition. **P*≤0.05, ***P*≤0.01, ****P*≤0.001, *****P*≤0.0001. IQR, interquartile range; MMR, DNA mismatch repair; UICC, Union Internationale Contre le Cancer.

Supplementary Files

This is a list of supplementary files associated with this preprint. Click to download.

- SupplementColonicIRChristiansenL.docx